



Quantitative and qualitative bone imaging: A review of synchrotron radiation microtomography analysis in bone research

Yoshihiro Obata^a, Hrishikesh A. Bale^b, Harold S. Barnard^c, Dula Y. Parkinson^c, Tamara Alliston^d, Claire Acevedo^{a,e,*}

^a Department of Mechanical Engineering, University of Utah, Salt Lake City, UT, 84112, USA

^b Carl Zeiss X-Ray Microscopy, Pleasanton, CA, 94588, USA

^c Advanced Light Source, Lawrence Berkeley Laboratory, Berkeley, CA, 94720, USA

^d Department of Orthopedic Surgery, University of California, San Francisco, CA, 94143, USA

^e Department of Biomedical Engineering, University of Utah, Salt Lake City, UT, 84112, USA

ARTICLE INFO

Keywords:

Bone
X-ray imaging
Synchrotron microtomography
Bone quality
Bone fragility
Toughness

ABSTRACT

All levels of the unique hierarchical structure of bone, consisting of collagen and hydroxyapatite crystals at the nanoscale to osteon/lamellae structures at the microscale, contribute to its characteristic toughness and material properties. Elements of bone's density and size contribute to bone quantity (or bone mass), whereas elements of bone's material composition, material properties, internal structure, and organization describe bone quality. Bone quantity and quality can be degraded by factors such as aging, disease, treatments, and irradiation, compromising its ability to resist fracture and sustain loading. Accessing the morphology and architecture of bone at the microscale to quantify microstructural features and assess the degree of mineralization and path of crack propagation in bone provides crucial information on how these factors are influencing bone quantity and quality. Synchrotron radiation micro-computed tomography (SR μ CT) was first used to assess bone structure at the end of the 1990's. One of the main advantages of the technique is that it enables accurate three-dimensional (3D), non-destructive quantification of structure while traditional histomorphometry on histological sections is inherently destructive to the sample and two-dimensional (2D). Additionally, SR μ CT uses monochromatic, high-flux X-ray beams to provide high-resolution and high-contrast imaging of bone samples. This allows the quantification of small microstructural features (e.g. osteocyte lacunae, canals, trabeculae, microcracks) and direct gray value compositional mapping (e.g. mineral quantification, cement lines) with greater speed and fidelity than lab-based micro-computed tomography. In this article, we review how SR μ CT has been applied to bone research to elucidate the mechanisms by which bone aging, disease, and other factors affect bone fragility and resistance to fracture.

1. Introduction

Biological materials often exhibit exceptional mechanical properties and intricate designs (Fratzl and Weinkamer, 2007). These designs are often organized hierarchically, where all structural levels contribute to the material properties at different length scales (Rho et al., 1998; Currey, 2005). Due to their unique properties, biological materials have inspired investigation from engineers and scientists, and bone is no exception (Fratzl, 2007; Wegst et al., 2015). The mechanical properties of bone are derived from its hierarchical, multi-scale arrangement of collagen molecules and hydroxyapatite crystals at nano-to macroscopic

dimensions (Rho et al., 1998; Zhang et al., 2003). At the microscopic level, mineralized collagen molecules and fibrils are organized in fiber patterns comprising the lamellar structure of the osteons in human cortical bone and the trabecular network in cancellous bone (Weiner et al., 1999). Osteons in cortical bone are cylindrical features 200–300 μ m in diameter containing a central longitudinal cavity called the Haversian canal (Fig. 1) (Zimmermann et al., 2016; Acevedo et al., 2015; Aizenberg et al., 2005). Trabeculae in cancellous bone comprise a three-dimensional (3D) porous network of processes with a 100–400 μ m thickness (Oftadeh et al., 2015). Features at all length scales in this complex, natural material account for bone's stiffness, strength, and

* Corresponding author. Department of Mechanical Engineering, University of Utah, Salt Lake City, UT, 84112, USA.

E-mail address: claire.acevedo@utah.edu (C. Acevedo).

<https://doi.org/10.1016/j.jmbbm.2020.103887>

Received 2 January 2020; Received in revised form 13 April 2020; Accepted 25 May 2020

Available online 25 June 2020

1751-6161/© 2020 Published by Elsevier Ltd.

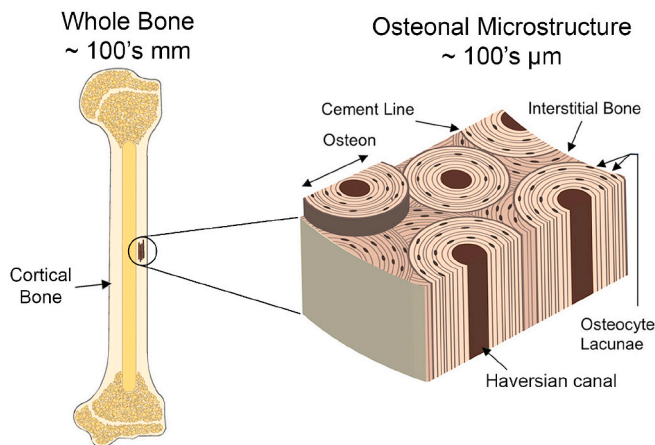


Fig. 1. Hierarchical structure of bone at the microscale. At the macroscale, human long bone consists of trabecular (cancellous) in the metaphysis and epiphysis regions and cortical bone in the diaphysis region. Secondary osteons (Haversian systems) in cortical bone are basic structural units at the microscale. Central to each osteon is a Haversian canal. These vascular porosities are connected to osteocytes in the Haversian system by canaliculi. Canaliculi are only observable at the nanoscale. Every osteocyte lies within small porosities called lacunae. At the boundary of each osteon is a highly mineralized cement line. (Figure adapted from Zimmermann et al. (2011); Milovanovic et al. (2013b); Acevedo et al. (2018b)).

toughness (Launey et al., 2010a).

In addition, bone is dynamic, constantly adapting to local needs and mechanical loading through remodeling (Nomura and Takano-Yamamoto, 2000; Huiskes et al., 2000). The remodeling cycle is a homeostatic process involving bone resorbing cells (osteoclast and osteocyte cells) and bone forming cells (osteoblast and osteocyte cells) (Yee et al., 2019; Milovanovic et al., 2013a). Because bone is continuously resorbed and reformed, bone quantity and quality are, by nature, dynamic. Bone quantity, also called bone mass or bone mineral density (BMD), is the amount of mineralized bone material in a given bone volume. Bone quantity relates to the degree of bone porosity, more specifically to the density and size of these porosities. Bone quality is used to describe bone material composition and material properties as well as bone microstructure and geometry, which affect whole bone's mechanical properties, such as strength and fracture resistance (Launey et al., 2010b; Schmidt et al., 2019). Although loss of bone resistance to fracture is often associated with low bone mass (Genant et al., 1999), over half of all non-vertebral fractures in people over 55 years of age occurred in those with a clinically normal bone mass (Schuit et al., 2004). Therefore, bone fragility is thought to result as well, from alterations in bone quality (Burr, 2004). Bone quality can be measured at the micro-scale through bone micro-architecture, mineral distribution linearly related to elastic properties, remodeling, and damage (Larue et al., 2011; Seeman, 2008).

Bone quality is compromised by age, bone fragility diseases (e.g. diabetes, osteogenesis imperfecta, and osteoporosis) or by treatments such as glucocorticoids, radiation, or long-term bisphosphonate use (Felsenberg and Boonen, 2005; Acevedo et al., 2018b; Grafe et al., 2014; O'Brien et al., 2004; Zimmermann et al., 2019; Barth et al., 2010). Although these diseases and aging are known contributors to poor bone quality, the underlying mechanisms controlling bone quality were not understood at the beginning of the 21st century, making the factors that regulate bone quality extensive topics of interest in the last twenty years (Zimmermann et al., 2015a; Acevedo et al., 2018a; Alliston, 2014). Synchrotron radiation micro-computed tomography (SR μ CT) techniques have provided major insight into volumetric bone structure and porosity, compositional mineral analysis, and crack path in bone fragility diseases. The first synchrotron imaging study dedicated to

trabecular bone was published in 1999 (Salomé et al., 1999). This study took advantage of the high resolution and high signal-to-noise ratio imaging provided by the monochromaticity and high-photon flux of X-ray synchrotron beam to image trabeculae. SR μ CT enables major advancements in the bone research field compared to other available techniques. Traditional techniques to characterize bone structure include histomorphometry based on histological sections and lab-based micro-computed tomography (μ CT) (Müller et al., 1998). Histomorphometry on 2D histological sections only provides 2D structural information of a specific cross-sectional area. Lab-based μ CT systems are widely used because of their accessibility. They have improved their efficiency and spatial resolution drastically over the last decades. However, their spatial resolution and the use of polychromatic energy above 30 keV limits their ability to image small microstructural features (e.g. osteocyte lacunae, canals, microcracks) and to perform direct gray value compositional mapping for mineral quantification. We are going to discuss three major advancements in understanding bone's resistance to fracture enabled by SR μ CT: namely quantification of 1) porosity and structure, 2) volumetric mineral distribution, and 3) crack deflection/twisting.

Porosity and structure. Size and density of porosities such as Haversian canals and osteocyte lacunae, as well as their organization in space (microstructure) are factors influencing both bone quantity and bone quality. Therefore, SR μ CT became a suitable tool for assessing bone quantity and quality (Gauthier et al., 2019; Withers, 2015; Donnelly, 2011). This method consists of taking transmission radiographs at multiple angles around an object and using them to reconstruct the inner microstructure of the object computationally (Hounsfield, 1973; Kak et al., 2002b). Inspection of bone matrix porosities and microstructure can reveal changes in their size and organization with disease that directly impact bone's ability to sustain loading and resist fracture.

Bone quality is also impacted by its ability to remodel at the cellular level (Alliston, 2014). Specific bone cells, called osteocytes, are embedded in bone matrix and have been revealed to play an integral role in bone remodeling (Bellido, 2014). Osteocytes orchestrate the actions of osteoclast and osteoblast cells and are responsible for periacicular remodeling (PLR)/pericanalicular remodeling and mechanotransduction (Bonewald, 2007, 2011; Dole et al., 2017). SR μ CT allows for quantification of osteocyte lacunae (i.e. the small space containing the osteocyte) size, density, and distribution to reveal remodeling activity and how osteocytes interact with the bone matrix to change bone microstructure. The study of bone fragility disease and treatments elucidates the normal mechanisms by which bone cells act to maintain biological and mechanical homeostasis in bone tissues (Dole et al., 2017; Acevedo et al., 2015). Indeed, because bone quality is a multiple length-scale dependent parameter that is heavily impacted by bone remodeling, analyzing these changes in microscale level features is an important strategy to better understand these intricate biological mechanisms and how their disruption compromises bone health.

Volumetric mineral distribution. If bone turnover performed by osteoclasts and osteoblasts is suppressed, excess mineralization of the bone matrix may occur. Regions of excess mineralization may act as a primary location for microcracking, resulting in fragile bone and ultimately impairing resistance to fracture that impedes crack growth (also called extrinsic mechanisms, see below) (Ettinger et al., 2013). Direct compositional measurement, such as mineral quantification, is one of the major advantages that SR μ CT offers over lab-based μ CT systems. The use of monochromatic (parallel beam) energy enables direct correlation between gray values and mineral attenuation. Change in volumetric tissue mineral density is useful to identify weak highly mineralized regions which are going to drive the crack extension.

Crack deflection/twisting. Bone fragility is associated with a major deterioration of bone toughness, or resistance to fracture (Inzana et al., 2013). Bone toughness results from the mutual competition of intrinsic mechanisms acting ahead of the crack tip, primarily at the nanoscale, and extrinsic mechanisms acting behind the crack tip at the microscale

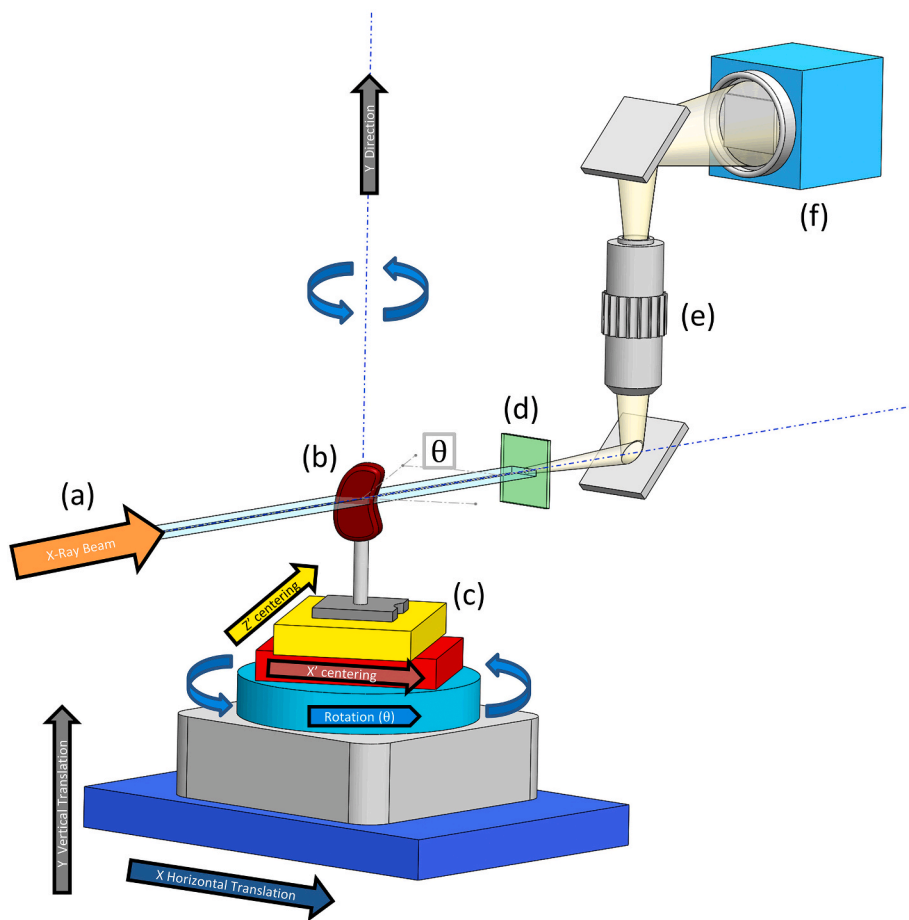


Fig. 2. SR μ CT scan geometry The X-ray beam (a) originating from the synchrotron source passes through the sample (b), creating a transmission image on the scintillator (d). The scintillator is crystalline material that converts the X-ray image into visible light which is then imaged directly with a conventional microscope objective (e) and a digital camera (f). The sample is mounted on top of precision stage (c), which used for positioning and alignment of the sample with respect to the beam and optics. The sample can then rotated and imaged over 180 or 360°.

(Launey and Ritchie, 2009; Zimmermann and Ritchie, 2015). Extrinsic mechanisms can be visualized via SR μ CT experiments; they act to impede crack growth by crack-tip shielding. These mechanisms include crack deflection/twisting and crack bridging (Peterlik et al., 2006; Ager et al., 2006; Nalla et al., 2005a; Ritchie et al., 2006). The concepts of extrinsic and intrinsic toughening mechanisms in bone and other materials has been pioneered by the Ritchie group at the University of California, Berkeley and Lawrence Berkeley National Laboratory.

Identifying changes in extrinsic (crack-tip shielding) toughness in bone necessitates the study of bone's microstructural features. Crack deflection and twisting in human cortical bone primarily occur at the cement line located at the interfaces of osteons (Yeni and Norman, 2000). The cement line is a highly mineralized region surrounding the secondary osteons in human bone (Nobakhti et al., 2014). Growing microcracks reaching these regions will be deflected and twisted to follow the path of least resistance offered by the cement lines (Zimmermann et al., 2009). Imaging both crack deflection/twisting and its position relative to cement lines has been made available with SR μ CT capabilities. In the case of murine bone, there are no osteons or Haversian canals, instead circumferential lamellae predominate (Saban et al., 1996). These lamellae layers in murine bone can act as delamination interfaces resulting in similar crack deflection and twisting (Carriero et al., 2014). This results in a tortuous crack path if a crack is propagating in the transverse (perpendicular to the longitudinal axis) direction, enhancing toughness in the transverse orientation in bone (Koester et al., 2011; Nalla et al., 2005b). SR μ CT visualization of three-dimensional crack profiles and their interaction with microstructural features is helpful in studying the origins of fracture resistance (Koester et al., 2008). Toughening mechanisms also exist in the longitudinal direction of bone via crack bridging, or uncracked-ligament

bridging (Nalla et al., 2004). This mechanism results in the creation of uncracked regions parallel to the crack path which carry the load that would otherwise contribute to further crack propagation (Zimmermann et al., 2011; Nalla et al., 2003). While this mechanism results in increased toughness in bone, crack bridging is not as influential as crack deflection and twist (Nalla et al., 2005b).

Here we review the current body of research on the applications of SR μ CT in providing quantitative and qualitative results to assess the mechanisms that control bone quantity and quality in bone fragility disease. Additionally, we will explain SR μ CT techniques and include a discussion on data acquisition and processing. Because of the advancements in computed tomography technology, the sophistication and capabilities of lab-based methods has increased in recent years. To address this, a comparison of different computed tomography methods is also performed. SR μ CT data has shown how healthy bone derives its unique fracture resistance and how it can be impaired by fragility diseases or treatment. Only SR μ CT can provide the three dimensional quantitative analysis of mineral density and the resolution to observe local changes in microstructure, bone matrix mineralization, and crack propagation. Finally, results from SR μ CT research between different studies analyzing bone disease, bone remodeling, and treatments will be compared.

2. Synchrotron microtomography image acquisition

Computed tomography (CT) is a 3D imaging process where many 2D X-ray images of a sample are acquired over a range of angles either over 180 or a complete 360° rotation, depending on the sample. These images are then used to computationally reconstruct a 3D volumetric image of the sample (Kak et al., 2002b; Bernhardt et al., 2004; Cano et al., 2008). CT imaging has broad applications in many fields that require the

non-destructive study of complex structures such as biological, medical, and materials sciences. CT scanners typically use conventional bremsstrahlung X-ray sources that generate X-rays by colliding a low energy (energy < 500 keV) electron beams into metallic targets. These sources are very compact (10s of centimeters in length) and are bright enough to be used in a variety of applications.

For CT with micro-scale resolution, μ CT, much brighter, higher flux X-ray beams are required. Because of the limits of X-ray source technology, lab-based conventional μ CT scanners require many hours per scan (du Plessis et al., 2016). For brighter beams and faster scans, SR μ CT is highly advantageous (See Fig. 2). Synchrotron radiation sources typically use large, circular electron accelerators (50–500m diameter) with high energy electron beams (energy: 1–10 GeV) (Barnard et al., 2017). Rather than colliding these electrons with targets, simply deflecting these beams by a few degrees with magnets causes synchrotron X-rays to be emitted. These X-ray beams are highly collimated, broad spectrum (spanning wide range of energy/wavelength), and are brighter than conventional X-ray sources by several orders of magnitude.

Due to the high X-ray flux, SR μ CT scans are regularly performed in several minutes with sub-micron resolution (Stampanoni et al., 2006). With optimization of image acquisition settings, images can be taken at rates faster than 1 image/second. The rapid scans that are achieved with SR μ CT are helpful for performing studies at reasonable timescales. Furthermore, they are necessary for studying biological samples because effects such as dehydration and changes in temperature over time can alter the dimensions of the sample, thus disturbing the CT scan process.

Depending on the source X-ray beam condition (i.e., either parallel beam or divergent cone beam geometry), the ultimate resolution achieved can change. In the case of parallel beam geometry typically used at many synchrotron light sources, the resolution is primarily dependent on the combination of scintillator properties, optical lens system, and detector (Carlton et al., 2016). In parallel beam geometry, the highest achievable resolution is typically limited by the wavelength of light produced in the scintillator and the visible light optics used for detection. When using a cone beam geometry, the resolution is dependent on the geometrical position of the detector from the source and sample, the source size and the camera pixel size (Langer et al., 2012b). Sometimes, cone beam geometries may combine scintillator coupled objectives for optical magnification such as in the laboratory X-ray microscopes (Feser et al., 2008). With cone beam, the highest achievable resolution is limited by the transverse size of the X-ray source.

The size of the field of view (FOV) that can be imaged is also an important consideration. For a given camera size, there is an inverse relationship between magnification and FOV. The other limitation on FOV is the X-ray beam size (typically several cm in width and several mm in height with the exact dimensions depending on the design of the X-ray beamline and synchrotron facility). For example, a typical SR μ CT instrument with a 10 \times objective and 0.6 micron resolution could image a 2 \times 2 mm² area FOV, corresponding to 2 mm (height) \times 2 mm (diameter) cylindrical volume. The same system with a lower magnification 2 \times objective with 3 micron resolution would be able to image a 10 \times 10 mm² FOV, corresponding to 10 mm (height) \times 10 mm (diameter) cylindrical volume. However, if the beam is only 5 mm tall this would limit the FOV in the latter case. For special cases where it is necessary to capture large samples or multi-scale structural features while maintaining high resolution, it is possible to increase the FOV with some additional complexity in the scan process. The height of the FOV can effectively be extended by taking multiple scans at different heights and stitching them together computationally. The width of the FOV can also be extended in the direction perpendicular to the axis of rotation by offsetting the axis of rotation and scanning over 360 $^\circ$, also called wide field view tomography (Labriet et al., 2018).

Synchrotron hard X-ray tomography beamlines provide a number of options for adjusting settings to optimize data collection for different applications. We will discuss three of these: monochromatic/

polychromatic X-ray energy, absorption or propagation-based phase contrast modes, and other scan parameters.

Monochromatic/Polychromatic X-ray energy. Synchrotrons produce very bright, broad spectrum X-rays, spanning a wide range of X-ray energy/wavelength. Many beamlines have an optical device called a monochromator that removes all but a narrow range of energy by preferentially reflecting X-rays of a specific energy/wavelength using a silicon crystal or multilayer mirror (somewhat similar to a diffraction grating in a spectrometer). The selected energy is dependent on the angle of the mirror and therefore the energy can be tuned for optimized contrast by tilting the mirror. Beamlines can switch between a polychromatic “white” or “pink” beam mode and a monochromatic mode by swapping the multilayer crystal in and out of the X-ray beam path. Most quantitative studies of bone using synchrotron sources rely on monochromatic radiation because the beam energy can be tuned to an energy that maximizes the absorption contrast and minimizes imaging artefacts. Moreover, the attenuation coefficients obtained from the scan data be more easily converted to quantitative values like mineral density, based on tabulated values of X-ray absorption for particular compounds at a given X-ray energy. Polychromatic scans with a synchrotron source have the advantage of higher flux and hence can be used for higher speed scanning. However, this mode is not as commonly used for bone due to additional radiation damage caused by significantly higher flux and the less optimized broad energy spectrum.

Absorption or propagation-based phase contrast modes. The most straightforward mechanism for X-ray imaging is absorption contrast. The density of a material and absorption properties of its constituent atoms are directly related to how many X-rays pass through the material to create an image. This is very effective for samples containing materials that have absorption properties that differ enough for them to be distinguished but are also close enough in absorption for either of the materials to be observed within the dynamic range of the detector. In the case of bone imaging, bone inherently has a good absorption contrast and is well suited for absorption contrast tomography. Moreover, a significant part of bone research studies involve measurement of changes in mineralization as a result of a drug or due to disease.

Synchrotron beamlines can also use multiple modes of phase contrast, including grating-based, speckle-based, and propagation-based. Propagation-based phase contrast is the simplest because it requires no additional hardware or different scanning routines (Paganin et al., 2002; De Witte et al., 2009). Phase contrast in this context occurs due to small variations in the refractive index of materials in the sample. Abrupt changes in refractive properties between structures in the sample causes the X-ray paths to be slightly deflected at material interfaces, producing fringes that tend to enhance edges. Grating-based phase contrast involves using two gratings: a phase grating to introduce a phase shift which through the Talbot effect creates intensity variations and a second grating to analyze the created pattern (Talbot, 1836; Momose et al., 2003). This type of phase contrast has been used in both lab-based settings and at synchrotron sources (Ruiz-Yaniz et al., 2016). Speckle-based phase contrast methods use a speckled surface, such as sandpaper or a biological membrane, with propagation-based methods to extract differential contrast in a scan; revealing information about the phase gradient (Morgan et al., 2012; Cerbino et al., 2008). Although the first uses of this technique were performed at synchrotron facilities, the technique has been expanded to lab-based CT setups as well (Zhou et al., 2015).

Phase contrast is particularly useful for imaging when materials have low absorption and cannot be easily distinguished from each other because of their similar absorption properties. The relative contribution of phase contrast to the image can be increased simply by moving the detector farther from the sample; with increasing distance of the detector, the phase fringe arising from transitions between regions with differing indices of refraction are better resolved and hence the boundaries separating the two regions are easily discerned. Due to the high coherence of synchrotron beams, samples that have lower

absorption contrast and are low absorbing produce excellent phase contrast. Because contrast is greatly dependent on the changes in the index of refraction rather than the X-ray absorption in phase contrast mode, features such as cracks, voids, and interface boundaries are clearly resolved.

Scan parameters. These parameters include exposure time, angular range of scanning and number of projection images collected over that range, whether the scan is done in “fly scan” mode (with the sample continuously rotated during scanning), and when and how many flat field (images without the sample) and dark field (images without X-ray illumination) images are collected. The major consideration in setting these parameters is the trade-off between scan time and image quality. Faster scans can help reduce delivered radiation dose or sample motion issues (mostly associated with dehydration in bone samples), but also have lower signal to noise due to few X-rays reaching the detector for each image. The process of optimizing these scan parameters is often closely tied to the image processing—the scans are often set to be run as fast as possible, to take advantage of limited synchrotron beam availability, while still enabling the image processing goals to be accomplished.

In addition to scan parameters, additional considerations must be made to account to irradiation of bone samples during scanning. This is usually the case when bone scans are taken in absorption mode to take advantage of the direct conversion of gray values into attenuation coefficients. In particular, *in situ* mechanical testing can expose bone to about 1 MGy of radiation. Ritchie and his group have shown that X-ray radiation, typically used in microtomography, degrades the mechanical properties of bone (Barth et al., 2010; Cornu et al., 2000). The total radiation dose need to be kept under 30 kGy to limit the detrimental effect of X-ray exposure (Barth et al., 2010, 2011). Decreases in ultimate strength, ductility, work-to-fracture, and fracture toughness were observed once the 30 kGy limit is reached (Barth et al., 2010). When comparing crack propagation in the transverse direction of bone using SR μ CT between low radiation dose and high dose, large deflections in the crack path are present in the low dose case while much lower severity deflection and twist are present in the high dose (Barth et al., 2011) indicative of toughness decrease. To decrease radiation dose when imaging a crack path, phase contrast mode is used to increase the sensitivity and contrast of a scan, enhancing the crack for a given radiation dose (Lewis, 2004). Managing radiation dose to mitigate alteration of bone properties is an important consideration to make when performing SR μ CT if mechanical testing is performed following a scan.

3. Synchrotron microtomography image processing

Following acquisition of SR μ CT data, tomographic slices must be reconstructed. In SR μ CT, X-ray projections of a sample being scanned are collected at multiple angles between 0 and 180 (or 360) degrees of rotation (MacDowell et al., 2016). A Fourier transform is performed on the projection data to obtain location estimates of the object’s Fourier transform in the frequency domain along radial lines (Smith, 2003). Ideally, the reconstruction of each projection angle could be summed to obtain information on the entire frequency domain to provide a complete, full reconstruction. However, this is not the case because each projection is only representative of a single radial line, resulting in features possessing a diffuse blur. To correct this blur, a filtered back-projection algorithm can be applied (Peters, 1997; Salomé et al., 1999). Filtered back-projection applies weighting to the frequency domain data, effectively allowing positive and negative components of the filtered projection to cancel during summing, and thereby eliminating the diffuse blur (Kak et al., 2002a). Commercial reconstruction software such as Octopus (Octopus v8; IIC UGent, Zwijnaarde) or python-based reconstruction through the TomoPy package relies on this image reconstruction method to obtain transverse slices relative to sample orientation during scanning (Gürsoy et al., 2014). Reconstructed data is processed using image processing tools, such as ImageJ (Rasband, W.S.,

ImageJ, US National Institutes of Health, Bethesda, <http://imagej.nih.gov/ij/>, 1997–2011.), Avizo (VSG, Visualization Sciences Group), and Dragonfly (ORS, Object Research Systems) to extract information about microstructure and crack propagation.

When processing SR μ CT data, artefacts from the scanning process must be removed to ensure accurate material characterization (Schlüter et al., 2014). To achieve the best possible accuracy, undesirable artefacts must be removed during or after reconstruction (Vidal et al., 2005). Additionally, proper segmentation techniques must be performed during image processing to accurately quantify bone (Dong et al., 2014). The main scanning artefacts that are present in SR μ CT data include stripe or ring artefacts, beam hardening, metal or attenuation coefficient artefacts, and shifted rotation center (Bouxsein et al., 2010). Stripes in the original, scanned data, which appear as rings in reconstructed data (Fig. 3a), are a result of inhomogeneous X-ray beam drift (Gürsoy et al., 2014). Defects on the scintillator or the detector of the synchrotron system can exacerbate these effects (Raven, 1998). This defect can be an issue because gray values of pixels/voxels can be altered and features of the microstructure can be obscured. To remove ring artefacts, combined wavelet-Fourier filtering is often implemented on the dataset before reconstruction to remove stripes (Münch et al., 2009).

Phase contrast can be a source of artefacts if it is not taken into account and images are assumed to be based purely on absorption (Vidal et al., 2005). In the context of SR μ CT, the type of phase-contrast that is contained in images is referred to as “propagation-based” phase contrast, and is a result of the scanned sample distorting the X-ray wavefront, causing edges and internal features of the bone to be highlighted with much higher or much lower intensity pixels than what is truly present (Fig. 3c) (Mayo et al., 2012). Not accounting for phase contrast contributions to images will lead to error when quantifying mineralization, also called volumetric tissue mineral density (vTMD), because pixel gray values are assumed to be directly related to levels of mineralization. The influence of phase contrast can interfere with detection of mineral heterogeneities that may be present at boundaries near pores in bone.

Phase retrieval techniques can be used to quantitatively reconstruct pixel gray values corresponding to the phase contrast. One popular approach to phase retrieval works by solving the ‘Transport of Intensity Equation’ (TIE) (Paganin et al., 2002). However, phase retrieval generally degrades image resolution, and is only quantitatively valid under assumptions that are often not met in bone samples (for example, that the sample is made of only one type of material).

While phase contrast can be problematic when studying vTMD, it can be beneficial - and in fact critical - in other bone and biological materials research. For instance, detecting microcracks and mapping out fracture in mechanically loaded bone samples, from either *in situ* or *ex situ* experiments is highly challenging especially when the cracks have not opened up sufficiently greater than the scan resolution (Larrue et al., 2011; Thurner et al., 2006). In such situations, the phase contrast mode is used. Phase-contrast signal from cracks arises quite strongly and highlights the cracks much more effectively (Sinnott-Jones et al., 2005). Segmenting the crack network is however not trivial when conventional thresholding methods or edge detection algorithms fail and may require manual to semi-automated or machine learning/deep learning segmentation (Liu et al., 2019; Zou et al., 2018; Wu et al., 2019).

Implanted objects, commonly metal, often have much higher linear attenuation coefficients (Akça and Erzeneoğlu, 2014). In a scan, these objects may cause total absorption of the X-ray, resulting in bright objects with star shaped reconstruction artefacts (Bouxsein et al., 2010). While metal artefacts in scans are greatly reduced with the use of synchrotron radiation, elimination of these artefacts can only presently be performed by removal of the object from the scan (Le Cann et al., 2019). Finally, detection of the proper center of rotation is necessary for a high-quality reconstructed dataset. Improper detection of a center of rotation results in obscured microstructural features during reconstruction (Fig. 3b). Center of rotation optimization is commonly

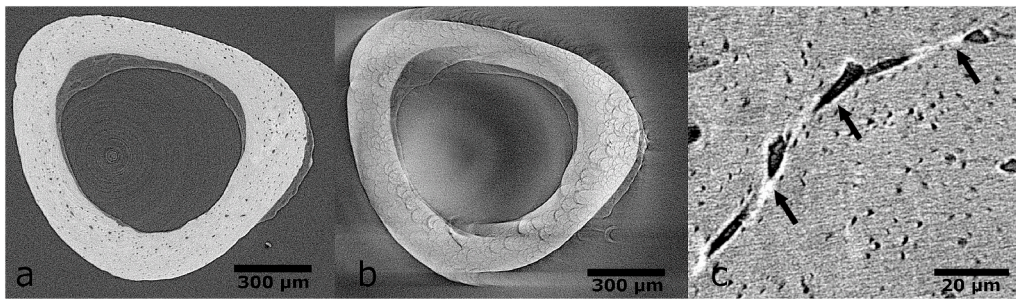


Fig. 3. Common artefacts present in SR μ CT scans. (a) Murine cortical bone cross-section. A ring artefact manifests itself as concentric circles about the rotation center in a scan. Often times these are the result of defects on the scintillator during scanning. (b) Murine cortical bone cross-section. Improper detection of the center of rotation during the image reconstruction process can result in undesirable center-of-rotation-shift artefacts, causing porosities and other microstructural features of bone to appear as crescent-shaped blurs. (c) Bovine cortical bone cross section. While still high resolution and relatively high quality, phase-contrast artefacts, indicated by black arrows, are present in the form of higher and lower intensity pixels around an edge or porosity in bone.

performed to detect and minimize these effects (Cheng et al., 2018).

After producing a high-quality reconstructed dataset devoid of artefacts, proper segmentation techniques must be applied to obtain characteristic results. In analysis of trabecular bone, the volume of interest can be selected by hand or can be separated from the bone using algorithms (Buie et al., 2007). In the quantification of SR μ CT data for cortical bone, segmentation is commonly performed to extract lacunar volume, canal diameter, orientation of microstructural features, examine crack propagation, or to find a host of other variables. Failure to accurately segment these features will result in a poor quantification on all successive analyses (Dong et al., 2014; Núñez et al., 2017; Carter et al., 2013). Various methods are used to segment lacunae and canals, but a large majority involve thresholding voxels within a certain range of gray value intensities and filtering a region based on appropriate particle size (Dong et al., 2014; Jameson et al., 2013; Jáuregui et al., 2016). Segmentation of cracks can be more challenging than osteocyte lacunae and vascular canals, but has been performed in several studies (Busse et al., 2013; Zimmermann et al., 2011; Acevedo et al., 2015; Zimmermann et al., 2015b). Segmentation of microcracks in bone using SR μ CT can prove even more difficult, as noise and artefacts from the scan obscure these features (Ma et al., 2016; Larrue et al., 2007). Despite this, some successful efforts have been made (Larrue et al., 2011).

4. SR μ CT and computed tomography in bone research

4.1. Computed tomography quantification parameters

While SR μ CT is a powerful method for investigating a variety of bone quantity and quality related parameters, it is not always the most appropriate computed tomography method. Depending on the parameters that are desired for a given study, different techniques, whether SR μ CT, lab-based μ CT, or synchrotron radiation nano-computed tomography (SRnCT), can be used to accomplish the task.

The technique chosen is often determined by the spatial resolution necessary to resolve key features. Choosing a technique which does not possess a high enough spatial resolution for a task will result in an inability to quantify parameters of interest. However, other factors will also influence the choice of the technique such as energy and flux range mostly suited to obtain high-contrast images and high signal-to-noise ratio in the material, or monochromaticity versus polychromaticity. Outlined in Table 1 are selected, common bone parameters quantified by computed tomography methods.

Bone quantity is assessed through parameters related to porosity size (Th, Dm, S, Ar, V) and density (Dn, N) since they evaluate the amount of

Table 1
Common micro-computed tomography parameters.

	Parameter	Description	Modality
Bone Quantity and Size Parameters	Tb.N	Trabecular Number	Lab μ CT, SR μ CT
	Tb.Th	Trabecular Thickness	Lab μ CT, SR μ CT
	BV/TV	Bone Volume Fraction	Lab μ CT, SR μ CT
	Ct.Th	Cortical Thickness	Lab μ CT, SR μ CT
	Ct.Ar	Cortical Area	Lab μ CT, SR μ CT
	Ca.Dm	Canal Diameter	SR μ CT, SRnCT
	Ca.Dn	Canal Density	SR μ CT
	Ct.Po	Cortical Porosity	SR μ CT
	Lc.V	Lacunar Volume	SR μ CT, SRnCT
	Lc.S	Lacunar Surface Area	SR μ CT, SRnCT
Bone Quality Parameters	Lc.Dn	Lacunar Density	SR μ CT, SRnCT
	Can.Dm ^a	Canalicular Diameter	SRnCT
	Can.N ^a	Canalicular Number	SRnCT
	Tb.Sp	Trabecular Separation	Lab μ CT, SR μ CT
	Ca.Sp	Trabecular Separation	Lab μ CT, SR μ CT
	TMD	Tissue Mineral Density	Lab μ CT (indirect), SR μ CT, SRnCT
	SMI	Structural Model Index	Lab μ CT, SR μ CT
	DA	Degree of Anisotropy	SR μ CT, SRnCT
	Ca.Conn	Canal Connectivity	SR μ CT, SRnCT
	Can.Conn ^a	Canalicular Connectivity	SRnCT

^a Canalicular variables are sometimes referred to with the abbreviation "Ca.", however, this work will use "Can." to distinguish this variable from canals.

bone volume fraction (BV/TV, Po). Bone quality's parameters involved structure and organization of material in space (Sp, SMI, DA), material composition (TMD), and osteocyte-mediated remodeling (Lc, Can).

TMD, or mineralization, is often reported as a mass of hydroxyapatite per volume or as a calcium percentage. The gray value, or voxel attenuation, of a reconstructed SR μ CT scan can be directly converted to vTMD values using the linear attenuation coefficient of the material being scanned (Nuzzo et al., 2002). This coefficient is dependent on the

Table 2

Comparison of lab-based μ CT and synchrotron-based μ CT. Relevant advantages and disadvantages of Lab μ CT and SR μ CT are shown for a variety of pertinent characteristics of each technique.

	Lab μ CT	SR μ CT
Resolution	<ul style="list-style-type: none"> Approaching approximately 0.5 μm through either detector-based or source-based system design (Zabler et al., 2020). Lab-based systems are also achieving nanoscale resolutions of 50 nm through the use of X-ray optics, such as Fresnel zone plate optics (Feser et al., 2008). 	<ul style="list-style-type: none"> Resolutions ranging from 30 nm to 0.5 μm are routinely achieved at synchrotron light sources using visible light optics or X-ray optics such as zone plates and compound reflective lenses (Weitkamp et al., 2010; Stampanoni et al., 2006).
Flux	<ul style="list-style-type: none"> Low flux (roughly three orders of magnitude lower than the flux in SRμCT). When lab-based systems try to push the flux through increase in power, there is an inevitable increase in spot size, leading to reduced resolution (Zabler et al., 2020). 	<ul style="list-style-type: none"> Synchrotron beamlines, especially ones with an associated insertion device, can deliver extremely high flux even at high resolutions (Weitkamp et al., 2010). The abundance of flux at synchrotron sources may inadvertently lead to sensitive samples receiving higher doses of radiation. This can change material properties, especially as seen in bone (Barth et al., 2010). Users can access lower side of the energy range, typically below 10 keV. These ranges are particularly well suited for obtaining higher contrast in biological samples.
Energy Range	<ul style="list-style-type: none"> Typically, lab-based systems can cover a much wider range of energies than SRμCT ranging from 30 keV to up to 650 keV. However, these systems cannot access some of the lower keV ranges necessary for biological samples. Also, lab sources tend to possess a nonlinear keV to flux behavior and generally have far lower flux at lower energies, resulting in great difficulty when performing in situ experiments on biological samples in a reasonable amount of time. 	<ul style="list-style-type: none"> Users can access lower side of the energy range, typically below 10 keV. These ranges are particularly well suited for obtaining higher contrast in biological samples.
Monochromaticity	<ul style="list-style-type: none"> LabμCT systems typically operate based on polychromatic X-ray sources and in general possess less tunability in scan energy compared to SRμCT. 	<ul style="list-style-type: none"> Single crystal multilayers allow for fine tuning of the source so that monochromatic X-rays of chosen energies are available. Choosing low energies can produce significantly higher contrast in samples such as bone where the differences in mineral density are relatively small (Stampanoni et al., 2006). Facilitates dual energy scanning approaches to take advantage of enhanced contrast at different energies from different constituents (Ito, 2005). No beam hardening artifacts are observed in scans utilizing monochromatic X-rays. Scintillators degrade faster due to higher flux. Scintillator degradation can lead to ring artefacts in the reconstructed 3D data. Secondly, most beamlines cater to a wide range of applications, requiring switching between a wide variety of experimental setups. These factors lead to a challenge in managing the scintillator optimizations that are key to ring artefact-free images.
Artefacts	<ul style="list-style-type: none"> Beam hardening artefacts are significantly present since there is higher absorption of lower energy X-rays leading to an artefact of higher intensity values on the edges of samples. Ring artefacts on LabμCT systems are also encountered but are more easily managed, especially because the scintillator or camera response does not change much over a period of time. 	<ul style="list-style-type: none"> One of the greatest advantages, among many others, of using synchrotron radiation for bone research. The grayscale value within a reconstructed volume directly corresponds to the attenuation coefficients of the minerals and constituents of the bone, hence the results can directly be used to correlate with other 2D mapping techniques (Bayat et al., 2005). Scan times typically range from a few seconds to tens of minutes depending on the mode and resolution of the measurement. High flux and advancements in sample stage and detector hardware have enables dynamic tomography with sufficiently high temporal resolution. Access to synchrotron facilities is limited. Beamtime is allocated through peer-review and open competition. Users have access to free but limited beamtime of usually a few 24-h beamtime shifts. In situ experiments need to be short due to limited beamtime access. Fast scan times enables in situ quasi-static and dynamic mechanical testing of materials. In situ environmental cells are usually an important part of synchrotron beamline programs. They are used to impose unique, controlled environmental conditions on samples such as different levels of temperature, pressure, humidity or vacuum.
Mineral Quantification (vTMD)	<ul style="list-style-type: none"> Grayscale values of reconstructed data do not directly correspond to attenuation coefficients. In order for a quantitative analysis of the mineral concentrations in bone, a calibration using known phantoms is required, involving additional steps and effort (Schweizer et al., 2007). 	<ul style="list-style-type: none"> One of the greatest advantages, among many others, of using synchrotron radiation for bone research. The grayscale value within a reconstructed volume directly corresponds to the attenuation coefficients of the minerals and constituents of the bone, hence the results can directly be used to correlate with other 2D mapping techniques (Bayat et al., 2005). Scan times typically range from a few seconds to tens of minutes depending on the mode and resolution of the measurement. High flux and advancements in sample stage and detector hardware have enables dynamic tomography with sufficiently high temporal resolution. Access to synchrotron facilities is limited. Beamtime is allocated through peer-review and open competition. Users have access to free but limited beamtime of usually a few 24-h beamtime shifts. In situ experiments need to be short due to limited beamtime access. Fast scan times enables in situ quasi-static and dynamic mechanical testing of materials. In situ environmental cells are usually an important part of synchrotron beamline programs. They are used to impose unique, controlled environmental conditions on samples such as different levels of temperature, pressure, humidity or vacuum.
Scan Times	<ul style="list-style-type: none"> Due to low flux, the scan times for a tomographic scan can range between 30 min and 10s of hours depending on the chosen resolution and sample size. 	<ul style="list-style-type: none"> Scan times typically range from a few seconds to tens of minutes depending on the mode and resolution of the measurement. High flux and advancements in sample stage and detector hardware have enables dynamic tomography with sufficiently high temporal resolution. Access to synchrotron facilities is limited. Beamtime is allocated through peer-review and open competition. Users have access to free but limited beamtime of usually a few 24-h beamtime shifts. In situ experiments need to be short due to limited beamtime access. Fast scan times enables in situ quasi-static and dynamic mechanical testing of materials. In situ environmental cells are usually an important part of synchrotron beamline programs. They are used to impose unique, controlled environmental conditions on samples such as different levels of temperature, pressure, humidity or vacuum.
Accessibility and cost	<ul style="list-style-type: none"> LabμCT systems are widely available and low cost. 	<ul style="list-style-type: none"> Access to synchrotron facilities is limited. Beamtime is allocated through peer-review and open competition. Users have access to free but limited beamtime of usually a few 24-h beamtime shifts. In situ experiments need to be short due to limited beamtime access. Fast scan times enables in situ quasi-static and dynamic mechanical testing of materials. In situ environmental cells are usually an important part of synchrotron beamline programs. They are used to impose unique, controlled environmental conditions on samples such as different levels of temperature, pressure, humidity or vacuum.
In situ experiments	<ul style="list-style-type: none"> LabμCT systems are geared towards long-duration in situ experiments due to longer scan times and better accessibility. 	<ul style="list-style-type: none"> In situ experiments need to be short due to limited beamtime access. Fast scan times enables in situ quasi-static and dynamic mechanical testing of materials. In situ environmental cells are usually an important part of synchrotron beamline programs. They are used to impose unique, controlled environmental conditions on samples such as different levels of temperature, pressure, humidity or vacuum.
Environmental chambers	<ul style="list-style-type: none"> Some manufacturers offer a range of environmental chambers and users may build their own as well for controlled, conventional purposes (in situ mechanical testing). A primary limitation of environmental chambers for LabμCT is space available for such a chamber. 	<ul style="list-style-type: none"> In situ environmental cells are usually an important part of synchrotron beamline programs. They are used to impose unique, controlled environmental conditions on samples such as different levels of temperature, pressure, humidity or vacuum.

X-ray energy, material, and material thickness used during scanning (Burghardt et al., 2007). Finite element models can be constructed from each SR μ CT scan. vTMD values of each voxel can then be assigned to a voxel-specific Young's modulus for each finite element using a power-law relationship (Wagner et al., 2011; Nyman et al., 2015; Easley et al., 2010; Wang et al., 2015).

Another advantage of high-quality images obtained by SR μ CT is the possibility to calculate reliable and precise measures of strain based on Digital Volume Correlation (DVC) (Gillard et al., 2014; Palanca et al., 2016). DVC can be applied to any 3D images of a material from a reference state to a deformed state in order to calculate the full 3D displacement and 3D strain maps. However, when strains obtained from SR μ CT are compared with the ones obtained from Lab μ CT, the error is reduced by one order of magnitude, and can therefore be used to evaluate strain in the physiological range (Palanca et al., 2017; Dall'Ara et al., 2014).

Canalicular diameter (Can.Dm), number (Can.N), and connectivity

(Can.Conn) are parameters that have been quantified using nano-tomography techniques in recent years. Due to the existence of canaliculi at the nanoscale in bone, extremely high resolutions are needed to visualize and quantify these structures. At this length scale, bone is studied at the cellular level using SRnCT, often with phase contrast (Peyrin et al., 2014a). SRnCT, with a typical resolution of 30–100 nm, is a powerful technique allowing for 3D visualization of bone ultrastructure (Langer et al., 2012b; Hesse et al., 2015b; Peyrin, 2009; Peyrin et al., 2014b), including canaliculi which were not previously visible with other forms of tomography (Langer et al., 2012a). However, the FOV, and thus the size of the sample, are reduced. For instance, a SRnCT scan with an image resolution of 50 nm implies approximately a $0.15 \times 0.15 \text{ mm}^2$ area FOV, corresponding to 0.15 mm (height) \times 0.15 mm (diameter) cylindrical volume. Quantification of the branching properties and number of canaliculi in relation to lacunae has been performed with SRnCT in addition to 3D visualization (Varga et al., 2015; Yu et al., 2020). Because of the increased resolution, highly localized effects can

be captured compared to SR μ CT. One such example is the mass density directly surrounding the lacunae and canaliculi. Gradients of this distribution are more pronounced near lacunae and diminish with age (Hesse et al., 2015a). With phase SRnCT, 3D organization of the mineralized collagen fibrils oscillations was revealed confirming fibril oscillations in a twisting plywood structure around osteons (Varga et al., 2013). Although SRnCT provides higher resolution images compared to SR μ CT, SRnCT possesses its own set of new challenges. While resolution is high using SRnCT, this comes at the expense of a smaller field of view when scanning the sample. SRnCT beamlines are more limited in their availability when compared to SR μ CT, which are also relatively limited compared to lab-based μ CT. The high resolutions of SRnCT scans are limited by the detector at the beamline as well as the radiation dose. Optimization of scanning parameters allows for simultaneous radiation dose reduction and higher signal to noise ratio (Pacureanu et al., 2012).

4.2. Differences between lab-based μ CT and SR μ CT

With the increasing power of lab-based μ CT, the capabilities of these systems and SR μ CT begin to overlap. New lab-based systems can resolve features at similar length scales to their synchrotron counterparts (0.5 μ m) via extremely small spot sizes, charged couple device cameras with smaller pixels, and high resolution scintillator-based magnification objectives. Additionally, lab-based systems are more compatible for experiments spanning a long duration of time due to limited synchrotron beamtime access. On the other hand, synchrotron sources have several key advantages over conventional μ CT and are user facilities which are free of cost if a beam time session is granted. Table 2 presents notable advantages and disadvantages of each method pertaining to significant factors of both techniques.

5. Application of SR μ CT in bone research

Trabecular bone's mechanical behavior is strongly influenced by microarchitectural features whereas cortical bone's mechanical behavior is primarily dominated by the material properties (Bayraktar et al., 2004; Burr, 2002). Bone is an organized multiscale arrangement of collagen and mineral at nano-to macroscopic dimensions. As such, it derives its unique mechanical properties over multiple length scales (Reznikov et al., 2014). At micron-scales, extrinsic toughening originates from the nature of the crack path in inducing crack deflection and bridging mechanisms (Nalla et al., 2005b). SR μ CT provides a unique, non-invasive means for 3D characterization of cracks and their interaction with the bone-matrix structure.

SR μ CT is powerful for the analysis of biological features in bone because it provides insight into both biological mechanisms and into the control of bone quality. The ability of SR μ CT to quantify thousands of lacunar volumes in 3D overcomes the limitations of more traditional histological approaches, in which analysis of lacunar size is time-consuming and based on a single 2D section through each lacunae. Quantification and visualization of the degree of mineralization, particularly around other biologically relevant features, can illuminate the mechanisms controlling matrix mineralization. Likewise, analysis of the size, tortuosity, and density of Haversian canals provides insight into bone vascularity and organization. Unfortunately, at this time, analysis of canalicular features is only possible with SRnCT. This information is incredibly valuable for understanding bone microstructure at even smaller length scales.

Ritchie and collaborators have used SR μ CT to understand how various biological factors can change the bone's complex structure and thereby affect its resistance to fracture. They found that bone's ability to resist crack propagation is affected by aging (Koester et al., 2011; Zimmermann et al., 2011), long-term bisphosphonate treatment (Acevedo et al., 2015), corticosteroid treatment (Fowler et al., 2017), vitamin-D deficiency (Busse et al., 2013), irradiation (Barth et al., 2010, 2011), as well as orientation (Koester et al., 2008) and multiaxial

loading (Zimmermann et al., 2009) with underlying biological and material mechanisms at the microstructural level observable with SR μ CT.

In addition, collaborations with the Alliston and Acevedo laboratories have revealed the critical role of osteocytes in PLR (Dole et al., 2017, 2019; Mazur et al., 2019; Fowler et al., 2017). By studying mice deficient in osteocyte-mediated PLR, these laboratories found that disruption of osteocyte remodeling function can cause a distinctive pattern of hypermineralization, as well as changes in osteocyte size and distribution, both of which are associated with bone fragility.

5.1. Microstructural features

Bone-embedded osteocytes account for 90%–95% of bone cells (Bonewald, 2011). Osteocytes connect with one another and with the vascular network through their dendritic processes, which extend through channels called canaliculi (Bonewald, 2006). Until recently, osteocytes were widely thought to lay relatively dormant in the bone matrix where they coordinated the activity of other cell types involved in bone remodeling. Osteocytes are now known to be responsible for localized bone remodeling through PLR remodeling as well as mechanotransduction (Qing et al., 2012; Klein-Nulend et al., 2005). During PLR, osteocytes dynamically remodel the lacuno-canalicular network through resorption and replacement of the surrounding bone matrix (Qing and Lynda, 2009; Dole et al., 2019). Mechanotransduction is the process of converting physical cues, such as fluid flow through canalicular networks, to biochemical signals that influence cellular behaviors, which can impact bone remodeling and other factors of bone homeostasis (Burger and Klein-Nulend, 1999).

Osteocyte cells themselves cannot be easily studied with SR μ CT, but SR μ CT analysis of their effects on the lacunae and bone matrix can provide insight into their remodeling function and agency on bone quality (Bonewald, 2011; Nicoletta et al., 2006; Gerbaix et al., 2017). Among the parameters that can be investigated using SR μ CT to elucidate osteocyte function are vTMD of bone, as well as lacunar volume, density, and orientation. Porosities in bone can be segmented by size and quantified to obtain information about lacunae.

Due to the relationship between osteocytes and PLR, suppression of PLR can appear in SR μ CT datasets as changes in lacunar size and orientation (Hesse et al., 2014b, 2015b; Roschger et al., 2019). The suppression of PLR through glucocorticoid-induced osteonecrosis reveals a decrease in lacunar volume in osteonecrotic bone compared to a non-treated, control bone. The significant change to both trabecular and cortical bone within 7 days of treatment extends surmounting evidence that PLR is indeed a dynamic process required for healthy bone homeostasis (Fowler et al., 2017).

Other agents that regulate cellular functions in bone also affect lacunar parameters in a variety of ways. While the precise causes of changes in osteocyte lacunar size and shape remain unanswered, it is clear that osteocytes dynamically respond to stimuli. Lacunar size is increased with a vitamin D deficiency, while lacunar density remained the same (Fig. 4) (Busse et al., 2013). Long-term glucocorticoid treatment has been shown to increase lacunar size (Lane and Yao, 2010). Lacunar size and density are additionally reported to vary with location, consistent with the anatomically distinct control of bone quality and PLR (Hesse et al., 2014a). SR μ CT revealed the osteocyte requirement for the enzyme MMP13 for PLR in long bones such as the femur and tibia (Mazur et al., 2019). It also demonstrated that cochlear bone maintains lacunar parameters independently of this protein. The extent to which the differential regulation of PLR is responsible for the dramatically different material properties in long bone and the cochlea remains to be fully elucidated. Nonetheless, analysis of these microstructural features in small bones from genetically modified mice is sufficient to reveal new biological mechanisms by which cochlear bone apparently suppress osteocyte-mediated PLR to protect hearing (Jáuregui et al., 2016).

The Haversian system, or secondary osteon, is comprised of a central

Haversian canal surrounded by concentric lamellae layers. The boundary of the Haversian system is marked by a highly mineralized cement line (Fig. 1) where microcracks often form. Because Haversian canals are vascular porosities, they can be identified by SR μ CT for three-dimensional visualization (Cooper et al., 2011). Efforts have also been made to visualize the canals with the surrounding osteon (Maggianno et al., 2016).

Simply visualizing Haversian canals is useful for qualitative analysis of bone quality in diseases such as Paget's disease of bone (PDB). One characteristic of this disease is hypervascularization (increased number or density of blood vessels) in bone and highly disorganized, immature lamellae surrounding disoriented Haversian canals (Zimmermann et al., 2015b). Vitamin D deficiency sees an increase in cortical porosity with a correlated increase in Haversian canal diameter (Busse et al., 2013). The effect of aging on Haversian canals has also been quantified using SR μ CT. Aged bone was noted to have three times the osteonal density, indicated by comparing young and aged Haversian canal density (Fig. 4) (Zimmermann et al., 2011). A higher density of Haversian canals implies an increase in the number of cement lines on osteonal boundaries. These hypermineralized cement lines have been shown to accumulate microcracks and deflect and twist the crack path.

5.2. Crack propagation and fracture

Healthy bone's unique ability to resist fracture is due in part to extrinsic toughness mechanisms at the microscale. However, these mechanisms can be impeded, resulting in bone fragility and increased risk of fracture. Aging has long been known to have a detrimental effect on toughness in bone due to decreasing bone mass, or quantity, with age,

but in the past two decades bone quality has emerged as an additional, potent source of bone degradation.

In the longitudinal direction of bone, presence of crack bridging is a driving mechanism of resistance to fracture. Crack bridges running parallel and forward of the crack tip act to carry load which would otherwise contribute to further propagating the crack. These bridges are observed to be smaller and less frequent in aged bone when compared to young bone (Zimmermann et al., 2011). Using SR μ CT, Haversian canal density, and thus osteonal density, is shown to be notably higher for aged bone (Fig. 4). The osteonal boundary possesses highly mineralized cement lines on which fracture can more easily propagate. While the osteonal boundary can possess beneficial microcracks that provide extrinsic toughening in bone, the smaller, less frequent microcracks due to aging, in combination with the increased potential surfaces for crack propagation in cement lines, result in the less tough, more brittle elderly bones. A reduction in the fracture toughness crack-resistance curve (or R-curve) slope for aged bone compared to young bone is in agreement with these mechanisms.

When a crack is propagating transversely to the osteon direction, crack deflection plays a dominant role in increasing extrinsic toughness at the microscale. While crack bridging primarily takes effect in the longitudinal direction of propagation along osteon boundaries, crack deflection acts most dominantly when cracks propagate in the transverse direction (Ritchie et al., 2009). This mechanism deflects, or changes the angle of, the direction of crack propagation from transverse to more longitudinal (Fig. 5). Again, osteons are key features for this mechanism in human bone, as crack deflection commonly occurs at the osteon boundary along cement lines where a path of least microstructural resistance is found. Because osteons are oriented longitudinally,

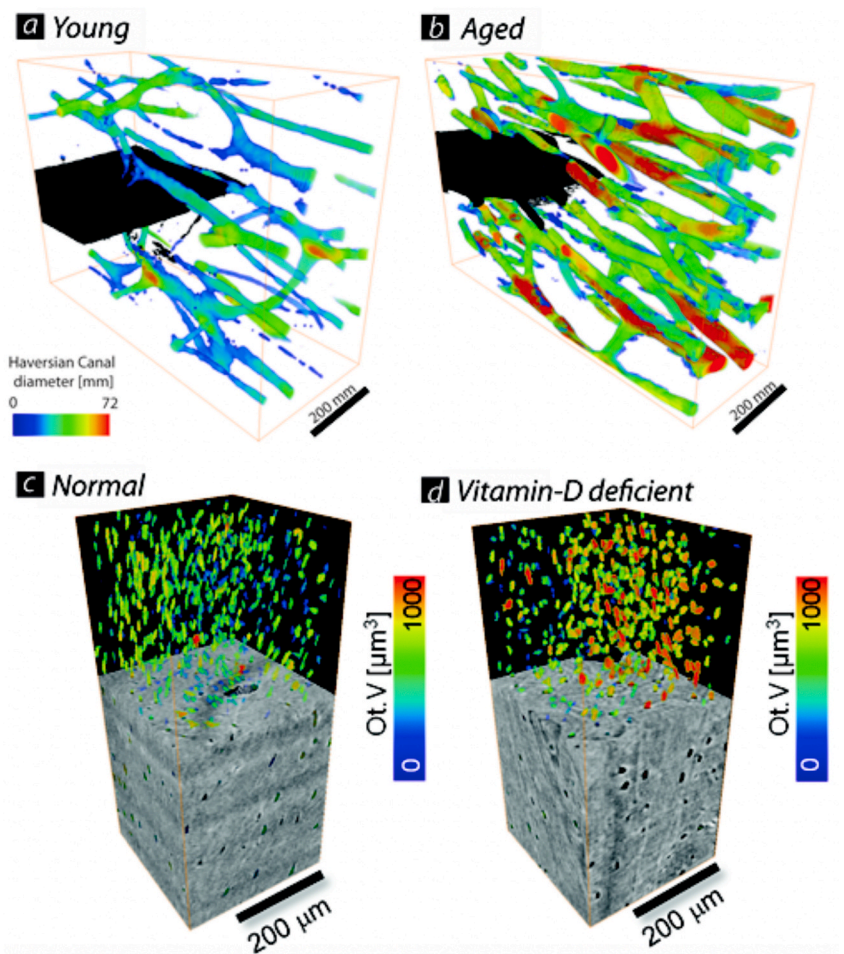


Fig. 4. Morphology changes due to aging and vitamin D deficiency. 3D images quantifying the size and distribution of Haversian canals in (a) young and (b) aged bone demonstrate how a higher density of canals and osteons with aging leads to a reduced toughness in the longitudinal orientation because there is more cement lines where microcracks can accumulate (Figure adapted from Zimmermann et al. (2011)). Vitamin D deficiency alters the morphology of bone causing larger osteocyte lacunae (c and d) (Figure adapted from Busse et al. (2013)).

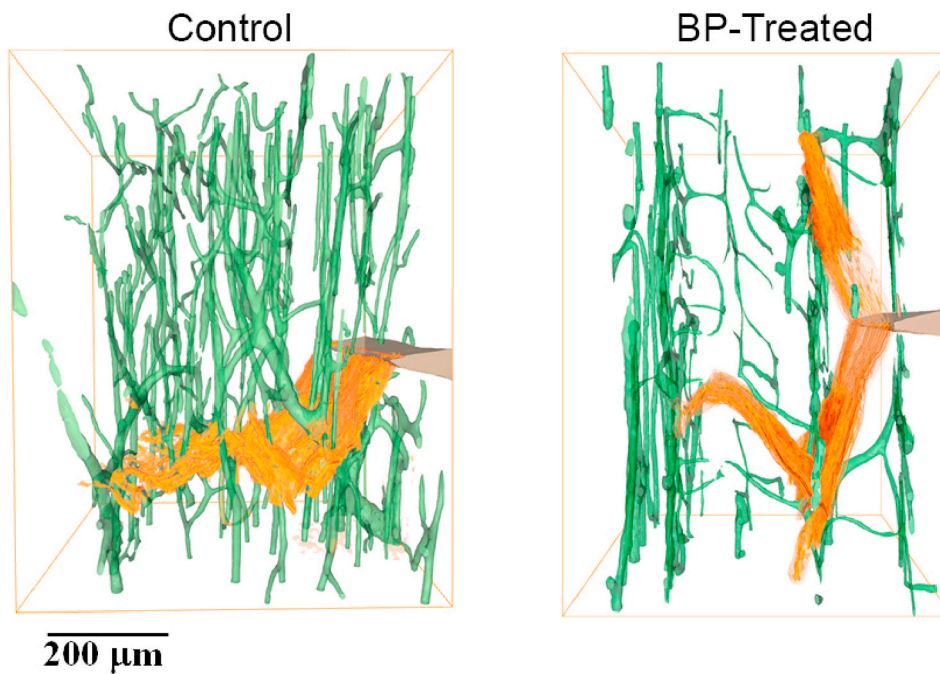


Fig. 5. Tomographic image showing the crack path from a notch oriented perpendicular to the osteonal orientation. Both control and bisphosphonate treated samples show the crack path (in orange) deflecting and twisting in relation to the bone's structure (i.e., specifically at the Haversian canals, which are shown in green) (Figure adapted from [Acevedo et al. Bone, 2015](#)).

toughness in the transverse direction is markedly higher (i.e. when the maximum driving force propagates the crack in the direction perpendicular to the osteons), by approximately five times more than in the longitudinal direction ([Koester et al., 2008](#)). In lamellar murine bone, crack deflection is also shown without the presence of osteons. In this case, the crack is deflected by the lamellae acting as delamination barriers to increase toughness ([Carriero et al., 2014](#)).

Crack deflection and toughness are often adversely impacted by bone disease, and SR μ CT has been used in combination with other techniques to elucidate mechanisms that affect toughness. Osteogenesis imperfecta (OI), brittle bone disease, is an ailment in which molecular level

mutations in bone are responsible for sudden whole-bone fracture ([Silence et al., 1979](#)). A comparison of crack path deflections in whole bone fracture from OI with healthy bone has revealed that wild-type, healthy bone crack propagation in the transverse direction has marked deflections and a tortuous crack path and OI has a characteristically smoother crack path ([Carriero et al., 2014](#)). In combination with R-curve analysis, it is clear that toughening mechanisms in OI bone are highly disrupted. When comparing healthy bone and PDB, crack growth of control bone displays large crack deflection at the longitudinally-oriented osteon boundaries, where PDB shows a distinctly straighter propagation in the transverse direction due partly

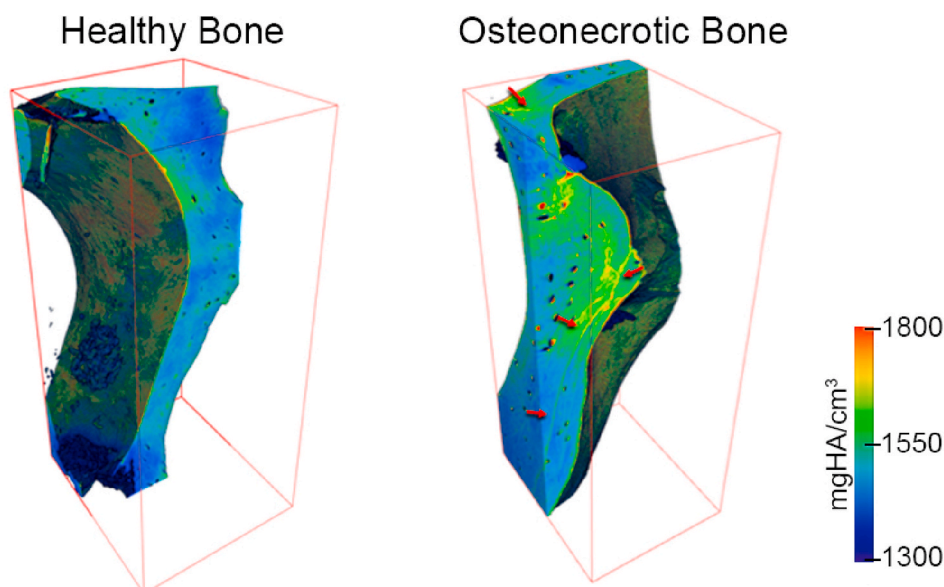


Fig. 6. Changes in mineralization due to glucocorticoid-induced osteonecrosis. Hypermineralization of osteonecrotic bone (arrows) compared to healthy bone from the human femoral head shows the role of perilacunar remodeling. (Figure adapted from [Fowler et al. Sci Rep, 2017](#)).

because of the previously mentioned disorganization of Haversian canals/osteons. Despite these features of the diseased bone, there is no significant difference in energy dissipation or crack-growth toughness between control and PDB samples. In the absence of crack deflection due to disorganization of the Haversian systems, increased plasticity of the bone and crack bridging have more pronounced effects, which partially compensate for the lack of crack deflection (Zimmermann et al., 2015b). The complexity of bone's hierarchical structure as well as the mechanisms that influence toughness in bone have profound effects on crack deflection.

5.3. Mineralization

vTMD is a component of bone quality made directly accessible using SR μ CT. When analyzing SR μ CT data for application in bone research, the shift in peak vTMD is studied as a measure of change in mineralization. The extremity regions of the mineralization curve can be indications of hypo- or hypermineralization, with an increased percentage of low mineralization values (low calcium weight percentage) indicating hypomineralization and an increased percentage of elevated mineralization values indicating hypermineralization. Because an average of the vTMD can normalize these differences, examining the distribution of mineralization is important. These mineralization parameters provide valuable information on the effects of disease or genetic modifications on the bone matrix. For example, in vitamin D deficient bone, a shift towards higher peak calcium weight percentage was observed with distinct regions of hypermineralization. Findings from this study indicate that a vitamin D deficiency may be related to macroscale loss of bone quality and increased fracture risk (Busse et al., 2013). In contrast, hypomineralization and a shift towards lower peak calcium weight percentage in PDB may partially be responsible for increased plasticity and a compensatory effect on bone fragility (Zimmermann et al., 2015b).

In some cases, hypermineralization is associated with alterations in osteocyte-mediated PLR and may be a potential contributor to bone fragility. The relationship between PLR and mineralization was investigated as part of a study evaluating glucocorticoid-induced osteonecrosis (Fig. 6). These studies highlight a major advantage of SR μ CT. Because of its ability to rapidly and precisely collect large amounts of quantitative data on mineralization and lacunar size, SR μ CT offers sensitivity that is currently available in no other technique. Although histological methods could not detect a glucocorticoid-dependent repression of PLR until 21 days of treatment, SR μ CT detected PLR suppression within 7 days of glucocorticoid treatment, with evidence of rapid hypermineralization and decreased lacunar size. Hypermineralization of the bone extracellular matrix likely contributed to bone fragility that causes the collapse of osteonecrotic subchondral bone and joint degredation (Fowler et al., 2017). PLR suppression is also apparent in osteoarthritis. Although previously thought to be a condition affecting primarily articular cartilage, a significant shift towards hypermineralization occurs in late-stage osteoarthritic bone, accompanying several other signs of PLR suppression. This observation suggests the important role of PLR in maintaining bone-cartilage crosstalk in healthy joints, and a mechanism by which PLR suppression in subchondral bone exacerbates joint disease (Mazur et al., 2019). Just as SR μ CT data was pivotal in revealing the role of osteocytes in joint disease, this approach has potential to make clear mechanisms contributing to a variety of pathological musculoskeletal conditions.

6. Closing remarks

Synchrotron radiation micro-computed tomography provides valuable quantitative and qualitative information on the internal morphology, mineralization, and crack path in bone. It does so through the reconstruction of high-quality image slices from scanned samples subjected to X-rays and is capable of resolving microscale-length

features. This reconstructed data can be processed to quantify porosity size and density in bone as an indicator of bone quantity, as well as structural, mineral composition (vTMD), and osteocyte lacunar quantification as indicators of bone quality. These parameters are but a few of the wide variety of information that can potentially be supplied through the use of SR μ CT (Table 1), and as synchrotron and lab-based CT techniques become more advanced, other mechanisms controlling bone quality are becoming more clear. Additionally, due to toughening mechanisms acting at every length-scale in the hierarchical structure of bone, examining features at the microscale assists in understanding the unique ability of bone to resist fracture and how this ability is degraded with disease. Because extrinsic toughening mechanisms such as crack deflection and twist occur predominantly at the microscale, SR μ CT is appropriately used to visualize and quantify crack deflection around highly mineralized regions.

Application of SR μ CT to assess bone quality and fracture mechanisms, particularly in unhealthy bone, is paramount for improving quality of life. No clear trends exist connecting bone fragility to lacunar size or density when studying PLR suppression through glucocorticoid-induced osteonecrosis, vitamin D deficiency, and cochlear bone with an MMP13 protease deficiency. This indicates that the factors responsible for controlling lacunar size and shape remain to be fully explored. Recent work in resistance to fracture does indicate that increased Haversian canal and osteonal density, in conjunction with larger and more frequent microcracks, contribute to lower toughness in aged bone due to a higher number of hypermineralized cement lines present for crack propagation to occur.

The longitudinally oriented cement lines in human bone and the lamellae layers in murine bone have been found to be the main source of crack deflection. Comparisons between healthy and fragile bones reveal that osteonal organization and mineralization of bone matrix play a large role in bone quality as well. Hypermineralization found in conditions such as OI and a vitamin D deficiency is thought to increase bone fragility, and hypomineralization is thought to contribute to the plasticity of bone seen in PDB. These applications showcase the diversity of SR μ CT and also display how research using SR μ CT has advanced understanding of bone quality through study of microstructure, fracture mechanisms, and mineralization.

Credit author statement

Yoshihiro Obata: Writing - Original Draft, Writing - Review & Editing **Hrishikesh A. Bale:** Writing - Review & Editing **Harold S. Barnard:** Writing - Review & Editing **Dula Y. Parkinson:** Writing - Review & Editing **Tamara Alliston:** Writing - Review & Editing **Claire Acevedo:** Writing - Original Draft, Writing - Review & Editing.

Declaration of competing interest

The authors declare that they have no known competing financial interests or personal relationships that could have appeared to influence the work reported in this paper.

Acknowledgments

This review article is written in honor of Dr. Robert O. Ritchie and his dedicated group over the last two decades, in recognition for his many important contributions to the field of fracture mechanics in bone. Dr. Ritchie's research addresses some of the most fundamental questions relating to measurement of toughness in bone, microstructural mechanisms by which bone resist fracture, visualization and quantification of bone microstructure using synchrotron X-ray radiation microtomography, and how X-ray irradiation alters bone's mechanical properties.

This work received support from the University of Utah seed grant (VPR Research Incentive 51900367 for YO), NIH (5R01DE019284-10

for TA) and DOE (DE-AC02-05CH11231 for DYP and HSB). This research used resources of the Advanced Light Source (mostly at beamline 8.3.2 - microtomography), a U.S. DOE Office of Science User Facility under contract no. DE-AC02-05CH11231.

References

- Acevedo, Claire, Bale, Hrishikesh, Gludovatz, Bernd, Amy, Wat, Tang, Simon Y., Wang, Mingyue, Busse, Björn, Zimmermann, Elizabeth A., Schaible, Eric, Allen, Matthew R., Burr, David B., Ritchie, Robert O., 2015. Alendronate treatment alters bone tissues at multiple structural levels in healthy canine cortical bone. *Bone* 81, 352–363. <https://doi.org/10.1016/j.bone.2015.08.002>, 87563282, URL.
- Acevedo, Claire, Stadelmann, Vincent A., Pioletti, Dominique P., Alliston, Tamara, Ritchie, Robert O., 2018a. Fatigue as the missing link between bone fragility and fracture. *Nature Biomedical Engineering* 2 (2), 62–71. <https://doi.org/10.1038/s41551-017-0183-9>, 2157846X, URL.
- Acevedo, Claire, Sylvia, Meghan, Schaible, Eric, Graham, James L., Stanhope, Kimber L., Metz, Lionel N., Gludovatz, Bernd, Schwartz, Ann V., Ritchie, Robert O., Alliston, Tamara N., Havel, Peter J., Fields, Aaron J., 2018b. Contributions of material properties and structure to increased bone fragility for a given bone mass in the UCD-T2DM rat model of type 2 diabetes. *J. Bone Miner. Res.* 33 (6), 1066–1075. <https://doi.org/10.1002/jbmr.3393>, 15234681.
- Ager III, W., Balooch, G., Ritchie, R.O., 2006. Fracture, aging, and disease in bone. *J. Mater. Res.* 21 (8), 1878–1892. <https://doi.org/10.1557/jmr.2006.0242>, 08842914.
- Aizenberg, Joanna, Weaver, James C., Thanawala, Monica S., Sundar, Vikram C., Morse, Daniel E., Fratzl, Peter, 2005. Materials science: skeleton of euleptella sp.: structural hierarchy from the nanoscale to the macroscale. *Science* 309 (5732), 275–278. <https://doi.org/10.1126/science.1112255>, 00368075.
- Akça, Burcu, Salih, Z., Erzenoğlu, 2014. The mass attenuation coefficients, electronic, atomic, and molecular cross sections, effective atomic numbers, and electron densities for compounds of some biomedically important elements at 59.5 keV. *Science and Technology of Nuclear Installations* 2014. <https://doi.org/10.1155/2014/901465>, 16876083.
- Alliston, Tamara, 2014. Biological regulation of bone quality. *Curr. Osteoporos. Rep.* 12 (3), 366–375. <https://doi.org/10.1007/s11914-014-0213-4>, 15442241.
- Barnard, Harold S., MacDowell, A.A., Parkinson, D.Y., Mandal, P., Czabaj, M., Gao, Y., Maillet, E., Blank, B., Larson, N.M., Ritchie, R.O., Gludovatz, B., Acevedo, C., Liu, D., 2017. Synchrotron X-ray micro-tomography at the advanced light source: developments in high-temperature in-situ mechanical testing. *J. Phys. Conf.* 849 (1) <https://doi.org/10.1088/1742-6596/849/1/012043>, 17426596.
- Barth, Holly D., Laune, Maximilien E., MacDowell, Alastair A., Ager, Joel W., Ritchie, Robert O., 2010. On the effect of X-ray irradiation on the deformation and fracture behavior of human cortical bone. *Bone* 46 (6), 1475–1485. <https://doi.org/10.1016/j.bone.2010.02.025>, 87563282, URL.
- Barth, Holly D., Zimmermann, Elizabeth A., Schaible, Eric, Tang, Simon Y., Alliston, Tamara, Ritchie, Robert O., 2011. Characterization of the effects of x-ray irradiation on the hierarchical structure and mechanical properties of human cortical bone. *Biomaterials* 32 (34), 8892–8904. <https://doi.org/10.1016/j.biomaterials.2011.08.013>, 01429612.
- Bayat, S., Apostol, L., Boller, E., Brochard, T., Peyrin, F., 2005. In vivo imaging of bone micro-architecture in mice with 3d synchrotron radiation micro-tomography. *Nucl. Instrum. Methods Phys. Res. Sect. A Accel. Spectrom. Detect. Assoc. Equip.* 548 (2–24), 247–252.
- Bayraktar, Harun H., Morgan, Elise F., Niebur, Glen L., Morris, Grayson E., Wong, Eric K., Keaveny, Tony M., 2004. Comparison of the elastic and yield properties of human femoral trabecular and cortical bone tissue. *J. Biomech.* 37 (1), 27–35. [https://doi.org/10.1016/S0021-9290\(03\)00257-4](https://doi.org/10.1016/S0021-9290(03)00257-4), 00219290.
- Bellido, Teresita, 2014. Osteocyte-driven bone remodeling. *Calcif. Tissue Int.* 94 (1), 25–34. <https://doi.org/10.1007/s00223-013-9774-y>, 0171967X.
- Bernhardt, Ricardo, Scharnweber, Dieter, Müller, Bert, Thurner, P., Schliephake, H., Wyss, P., Beckmann, F., Goebels, Jürgen, Worch, H., 2004. Comparison of microfocus- and synchrotron x-ray tomography for the analysis of osteointegration around t6al4v implants. *Eur. Cell. Mater.* 7 (42), e51.
- Bonewald, Lynda F., 2006. Mechanosensation and transduction in osteocytes. *BoneKey-Osteovision* 3 (10), 7.
- Bonewald, L.F., 2007. Osteocytes as dynamic multifunctional cells. *Ann. New York Acad. Sci.* 1116 (1), 281–290.
- Bonewald, L.F., 2011. The amazing osteocyte. *J. Bone Mineral Res.* 26 (2), 229–238. Vancouver.
- Bouxsein, Mary L., Boyd, Stephen K., Christiansen, Blaine A., Guldberg, Robert E., Jepsen, Karl J., Müller, Ralph, 2010. Guidelines for assessment of bone microstructure in rodents using micro-computed tomography. *J. Bone Miner. Res.* 25 (7), 1468–1486.
- Buie, Helen R., Campbell, Graeme M., Klinck, R. Joshua, MacNeil, Joshua A., Boyd, Steven K., 2007. Automatic segmentation of cortical and trabecular compartments based on a dual threshold technique for in vivo micro-CT bone analysis. *Bone* 41 (4), 505–515. <https://doi.org/10.1016/j.bone.2007.07.007>, 87563282.
- Burger, E.H., Klein-Nulend, J., 1999. Mechanotransduction in bone - role of the lacuno-canalicular network. *FASEB (Fed. Am. Soc. Exp. Biol.) J.* 13 (8 Suppl. L), 101–112, 08926638.
- Burghardt, Andrew J., Wang, Yongmei, Elalieh, Hashem, Thibault, Xavier, Bikle, Daniel, Peyrin, Françoise, Majumdar, Sharmila, 2007. Evaluation of fetal bone structure and mineralization in IGF-I deficient mice using synchrotron radiation microtomography and Fourier transform infrared spectroscopy. *Bone* 40 (1), 160–168. <https://doi.org/10.1016/j.bone.2006.06.017>, 87563282.
- Burr, D.B., 2002. The contribution of the organic matrix to bone's material properties. *Bone* 31 (1), 8–11. [https://doi.org/10.1016/S8756-3282\(02\)00815-3](https://doi.org/10.1016/S8756-3282(02)00815-3), 87563282, URL.
- Burr, D.B., 2004. Bone quality: Understanding what matters. *Journal of Musculoskeletal Neuronal Interactions* 4 (2), 184–186.
- Busse, Björn, Bale, Hrishikesh A., Zimmermann, Elizabeth A., Panganiban, Brian, Barth, Holly D., Carriero, Alessandra, Vettorazzi, Eik, Zustin, Josef, Hahn, Michael, Ager, Joel W., Püschel, Klaus, Amling, Michael, Robert, O., Ritchie, 2013. Vitamin D deficiency induces early signs of aging in human bone, increasing the risk of fracture. *Sci. Transl. Med.* 5 (193) <https://doi.org/10.1126/scitranslmed.3006286>, 19466234.
- Cano, Jorge, Campo, Julián, Vaquero, Juan José, Martínez-González, Jose María, Bascones, Antonio, et al., 2008. High resolution image in bone biology ii. review of the literature. *Med. Oral, Patol. Oral Cirugía Bucal* 13 (1), 31.
- Carlton, Holly D., Elmer, John W., Li, Yan, Pacheco, Mario, Goyal, Deepak, Parkinson, Dilworth Y., MacDowell, Alastair A., 2016. Using synchrotron radiation microtomography to investigate multi-scale three-dimensional microelectronic packages. *JoVE* (110), e53683.
- Carriero, Alessandra, Zimmermann, Elizabeth A., Paluszny, Adriana, Tang, Simon Y., Bale, Hrishikesh, Busse, Björn, Alliston, Tamara, Kazakia, Galateia, Ritchie, Robert O., Shefelbine, Sandra J., 2014. How tough is brittle bone? Investigating osteogenesis imperfecta in mouse bone. *J. Bone Miner. Res.* 29 (6), 1392–1401. <https://doi.org/10.1002/jbmr.2172>, 15234681.
- Carter, Yasmin, David, C., Thomas, L., Clement, John G., Peele, Andrew G., Hannah, Kevin, Cooper, David M.L., 2013. Variation in osteocyte lacunar morphology and density in the human femur - a synchrotron radiation micro-CT study. *Bone* 52 (1), 126–132. <https://doi.org/10.1016/j.bone.2012.09.010>, 87563282, URL.
- Cerbino, R., Peverini, L., MAC Potenza, Robert, A., Bösecke, P., Giglio, M., 2008. X-ray scattering information obtained from near-field speckle. *Nat. Phys.* 4 (3), 238–243.
- Chang, Chieh Cheng, Yu Tai, Ching, Pai Hung, Ko, Yeukuang, Hwu, 2018. Correction of center of rotation and projection angle in synchrotron X-ray computed tomography. *Sci. Rep.* 8 (1), 1–9. <https://doi.org/10.1038/s41598-018-28149-8>, 20452322, URL.
- Cooper, D.M.L., Erickson, B., Peele, A.G., Hannah, K., Thomas, C.D.L., Clement, J.G., 2011. Visualization of 3D osteon morphology by synchrotron radiation micro-CT. *J. Anat.* 219 (4), 481–489. <https://doi.org/10.1111/j.1469-7580.2011.01398.x>, 00218782.
- Cornu, O., Banse, X., Docquier, P.L., Luyckx, S., Delloye, Ch, 2000. Effect of freeze-drying and gamma irradiation on the mechanical properties of human cancellous bone. *J. Orthop. Res.* 18 (3), 426–431. <https://doi.org/10.1002/jor.1100180314>, 07360266.
- Currey, John D., 2005. Hierarchies in biomineral structures. *Science* 309 (5732), 253–254. <https://doi.org/10.1126/science.1113954>, 00368075.
- Dall'Ara, E., Barber, D., Viceconti, M., 2014. About the inevitable compromise between spatial resolution and accuracy of strain measurement for bone tissue: a 3d zero-strain study. *J. Biomech.* 47 (12), 2956–2963.
- De Witte, Yoni, Boone, Matthieu, Vlassenbroeck, Jelle, Dierick, Manuel, Van Hoorebeke, Luc, 2009. Bronnikov-aided correction for x-ray computed tomography. *JOSA A* 26 (4), 890–894.
- Dole, Neha S., Mazur, Courtney M., Acevedo, Claire, Lopez, Justin P., Monteiro, David A., Fowler, Tristan W., Gludovatz, Bernd, Walsh, Flynn, Regan, Jenna N., Messina, Sara, Evans, Daniel S., Lang, Thomas F., Zhang, Bin, Ritchie, Robert O., Mohammad, Khalid S., Alliston, Tamara, 2017. Osteocyte-intrinsic TGF- β signaling regulates bone quality through perilacunar/canalicular remodeling. *Cell Rep.* 21 (9), 2585–2596. <https://doi.org/10.1016/j.celrep.2017.10.115>, 22111247, URL.
- Dole, Neha S., Yee, Cristal S., Mazur, Courtney M., 2019. Claire Acevedo, and Tamara Alliston. Tgfb β Regulation of Perilacunar/canalicular Remodeling Is Sexually Dimorphic. *bioRxiv*. <https://doi.org/10.1101/737395>. URL: <https://www.biorxiv.org/content/early/2019/08/16/737395>.
- Dong, Pei, Hauptert, Sylvain, Hesse, Bernhard, Langer, Max, Gouttenoire, Pierre Jean, Bousson, Valérie, Peyrin, Françoise, 2014. 3D osteocyte lacunar morphometric properties and distributions in human femoral cortical bone using synchrotron radiation micro-CT images. *Bone* 60, 172–185. <https://doi.org/10.1016/j.bone.2013.12.008>, 87563282, URL.
- Donnelly, Eve, 2011. Methods for assessing bone quality: a review. *Clin. Orthop. Relat. Res.* 469 (8), 2128–2138. <https://doi.org/10.1007/s11999-010-1702-0>, 15281132.
- du Plessis, Anton, Gerhard le Roux, Stephan, Guelpa, Anina, 2016. The ct scanner facility at stellenbosch university: an open access x-ray computed tomography laboratory. *Nucl. Instrum. Methods Phys. Res. Sect. B Beam Interact. Mater. Atoms* 384, 42–49.
- Easley, Sarah K., Jekir, Michael G., Burghardt, Andrew J., Li, Mei, Keaveny, Tony M., 2010. Contribution of the intra-specimen variations in tissue mineralization to pth-and raloxifene-induced changes in stiffness of rat vertebrae. *Bone* 46 (4), 1162–1169.
- Ettinger, B., Burr, D.B., Ritchie, R.O., 2013. Proposed pathogenesis for atypical femoral fractures: lessons from materials research. *Bone* 55 (2), 495–500. <https://doi.org/10.1016/j.bone.2013.02.004>, 87563282, URL.
- Felsenberg, Dieter, Boonen, Steven, 2005. The bone quality framework: determinants of bone strength and their interrelationships, and implications for osteoporosis management. *Clin. Therapeut.* 27 (1), 1–11. <https://doi.org/10.1016/j.clinthera.2004.12.020>, 1879114X.
- Feser, M., Gelb, J., Chang, H., Cui, H., Diewer, F., Lau, S.H., Tkachuk, A., Yun, W., 2008. Sub-micron resolution ct for failure analysis and process development. *Meas. Sci. Technol.* 19 (9), 094001.

- Fowler, Tristan W., Acevedo, Claire, Mazur, Courtney M., Hall-Glenn, Faith, Fields, Aaron J., Bale, Hrishikesh A., Ritchie, Robert O., Lotz, Jeffrey C., Vail, Thomas P., Alliston, Tamara, 2017. Glucocorticoid suppression of osteocyte perilacunar remodeling is associated with subchondral bone degeneration in osteonecrosis. *Sci. Rep.* 7 (February), 1–13. <https://doi.org/10.1038/srep44618>, 20452322, URL.
- Fratzl, Peter, 2007. Biomimetic materials research: what can we really learn from nature's structural materials? *J. R. Soc. Interface* 4 (15), 637–642. <https://doi.org/10.1098/rsif.2007.0218>, 17425662.
- Fratzl, Peter, Weinkamer, Richard, 2007. Nature's hierarchical materials. *Prog. Mater. Sci.* 52 (8), 1263–1334.
- Gauthier, Rémy, Follet, Hélène, Olivier, Cécile, Mitton, David, Peyrin, Françoise, 2019. 3D analysis of the osteonal and interstitial tissue in human radii cortical bone. *Bone* 127 (January), 526–536. <https://doi.org/10.1016/j.bone.2019.07.028>, 87563282, URL.
- Genant, Harry K., Cooper, Cyrus, Poor, Gyula, Reid, Ian, Ehrlich, George, Kanis, J., Christopher Nordin, B.E., Barrett-Connor, Elizabeth, Black, Dennis, Bonjour, J.-P., et al., 1999. Interim report and recommendations of the world health organization task-force for osteoporosis. *Osteoporos. Int.* 10 (4), 259–264.
- Gerbaix, Maude, Gnyubkin, Vasily, Farlay, Delphine, Olivier, Cécile, Ammann, Patrick, Courbon, Guillaume, Laroche, Norbert, Genthial, Rachel, Follet, Hélène, Peyrin, Françoise, Shenkman, Boris, Gauquelin-Koch, Guillemette, Vico, Laurence, 2017. One-month spaceflight compromises the bone microstructure, tissue-level mechanical properties, osteocyte survival and lacunae volume in mature mice skeletons. *Sci. Rep.* 7 (1), 2659. <https://doi.org/10.1038/s41598-017-03014-2>, 20452322.
- Gillard, F., Boardman, Richard, Mavrogordato, Mark, Hollis, Dave, Sinclair, Ian, Pierron, Fabrice, Browne, Martin, 2014. The application of digital volume correlation (dvc) to study the microstructural behaviour of trabecular bone during compression. *Journal of the mechanical behavior of biomedical materials* 29, 480–499.
- Grafé, Ingo, Yang, Tao, Alexander, Stefanie, Homan, Erica P., Lietman, Caressa, Jiang, Ming Ming, Bertin, Terry, Munivez, Elda, Chen, Yuqing, Dawson, Brian, Ishikawa, Yoshihiro, Weis, Mary Ann, Kuber Sampath, T., Ambrose, Catherine, Eyre, David, Bächinger, Hans Peter, Lee, Brendan, 2014. Excessive transforming growth factor- β 2 signaling is a common mechanism in osteogenesis imperfecta. *Nat. Med.* 20 (6), 670–675. <https://doi.org/10.1038/nm.3544>, 1546170X.
- Gürsoy, Doğa, De Carlo, Francesco, Xiao, Xianghui, Jacobsen, Chris, 2014. TomoPy: a framework for the analysis of synchrotron tomographic data. *J. Synchrotron Radiat.* 21 (5), 1188–1193. <https://doi.org/10.1107/S1600577514013939>, 16005775.
- Hesse, Bernhard, Langer, Max, Varga, Peter, Pacureanu, Alexandra, Dong, Pei, Schrof, Susanne, Manünicke, Nils, Suhonen, Heikki, Olivier, Cecile, Maurer, Peter, Kazakia, Galateia J., Kay, Raum, Peyrin, Françoise, 2014a. Alterations of mass density and 3D osteocyte lacunar properties in bisphosphonate-related osteonecrotic human jaw bone, a synchrotron μ CT study. *PLoS One* 9 (2), 1–11. <https://doi.org/10.1371/journal.pone.0088481>, 19326203.
- Hesse, Bernhard, Maennicke, Nils, Pacureanu, Alexandra, Varga, Peter, Langer, Max, Maurer, Peter, Peyrin, Françoise, Kay, Raum, 2014b. Accessing osteocyte lacunar geometrical properties in human jaw bone on the submicron length scale using synchrotron radiation μ CT. *J. Microsc.* 255 (3), 158–168.
- Hesse, Bernhard, Varga, Peter, Langer, Max, Pacureanu, Alexandra, Schrof, Susanne, Männicke, Nils, Suhonen, Heikki, Maurer, Peter, Cloetens, Peter, Peyrin, Françoise, et al., 2015a. Canalicular network morphology is the major determinant of the spatial distribution of mass density in human bone tissue: evidence by means of synchrotron radiation phase-contrast nano-ct. *J. Bone Miner. Res.* 30 (2), 346–356.
- Hesse, Bernhard, Varga, Peter, Langer, Max, Pacureanu, Alexandra, Schrof, Susanne, Männicke, Nils, Suhonen, Heikki, Maurer, Peter, Cloetens, Peter, Peyrin, Françoise, et al., 2015b. Canalicular network morphology is the major determinant of the spatial distribution of mass density in human bone tissue: evidence by means of synchrotron radiation phase-contrast nano-ct. *J. Bone Miner. Res.* 30 (2), 346–356.
- Hounsfield, Godfrey N., 1973. Computerized transverse axial scanning (tomography): Part 1. description of system. *Br. J. Radiol.* 46 (552), 1016–1022.
- Huiskes, Rik, Rulmerman, Ronald, Harry Van Lenthe, G., Janssen, Jan D., 2000. Effects of mechanical forces on maintenance and adaptation of form in trabecular bone. *Nature* 405 (6787), 704–706. <https://doi.org/10.1038/35015116>, 00280836.
- Inzana, Jason A., Maher, Jason R., Takahata, Masahiko, Schwarz, Edward M., Berger, Andrew J., Awad, Hani A., 2013. Bone fragility beyond strength and mineral density: Raman spectroscopy predicts femoral fracture toughness in a murine model of rheumatoid arthritis. *J. Biomech.* 46 (4), 723–730. <https://doi.org/10.1016/j.jbiomech.2012.11.039>, 00219290, URL.
- Ito, Masako, 2005. Assessment of bone quality using micro-computed tomography (micro-ct) and synchrotron micro-ct. *J. Bone Miner. Metabol.* 23 (1), 115–121.
- Jameson, John R., Albert, Carolyne I., Busse, Bjoern, Smith, Peter A., Harris, Gerald F., 2013. 3D micron-scale imaging of the cortical bone canal network in human osteogenesis imperfecta (OI). In: *Medical Imaging 2013: Biomedical Applications in Molecular, Structural, and Functional Imaging*, 8672(March 2013):86721L. <https://doi.org/10.1117/12.2007209>, 16057422.
- Jáuregui, Emmanuel J., 2016. Omar akil, Claire Acevedo, faith Hall-glenn, betty S. Tsai, Hrishikesh A. Bale, ellen liebenberg, mary beth humphrey, robert O. Ritchie, lawrence R. Lustig, and Tamara Alliston. Parallel mechanisms suppress cochlear bone remodeling to protect hearing. *Bone* 89 (7–15). <https://doi.org/10.1016/j.bone.2016.04.010>, 87563282, URL.
- Kak, Avinash C., Slaney, Malcolm, Wang, Ge, 2002a. Principles of computerized tomographic imaging. *Med. Phys.* 29 (1), 107–107.
- Kak, Avinash C., Slaney, Malcolm, Wang, Ge, 2002b. Principles of computerized tomographic imaging. *Med. Phys.* 29 (1), 107–107.
- Klein-Nulend, Jenneke, Vatsa, Aviral, Bacabac, Rommel G., Tan, S. Djien, Smit, Theo H., 2005. The role of osteocytes in bone mechanotransduction. *Curr. Opin. Orthop.* 16 (5), 316–324. <https://doi.org/10.1097/01.bco.0000177409.72833.ba>, 10419918.
- Koester, K.J., Ager, J.W., Ritchie, R.O., 2008. The true toughness of human cortical bone measured with realistically short cracks. *Nat. Mater.* 7 (8), 672–677. <https://doi.org/10.1038/nmat2221>, 14764660.
- Koester, K.J., Barth, H.D., Ritchie, R.O., 2011. Effect of aging on the transverse toughness of human cortical bone: evaluation by R-curves. *Journal of the Mechanical Behavior of Biomedical Materials* 4 (7), 1504–1513. <https://doi.org/10.1016/j.jmbm.2011.05.020>, 17516161, URL.
- Labriet, H., Nemoz, C., Renier, M., Berkvens, P., Brochard, T., Cassagne, R., Elleaume, Hélène, Estève, François, Verry, Camille, Balosso, Jacques, et al., 2018. Significant dose reduction using synchrotron radiation computed tomography: first clinical case and application to high resolution ct exams. *Sci. Rep.* 8 (1), 1–7.
- Lane, Nancy E., Yao, Wei, 2010. Glucocorticoid-induced bone fragility: new insights. *Ann. N. Y. Acad. Sci.* 1192, 81–83. <https://doi.org/10.1111/j.1749-6632.2009.05228.x>, 17496632.
- Langer, Max, Pacureanu, Alexandra, Suhonen, Heikki, Grimal, Quentin, Cloetens, Peter, Peyrin, Françoise, 2012a. X-ray phase nanotomography resolves the 3D human bone ultrastructure. *PLoS One* 7 (8), 1–7. <https://doi.org/10.1371/journal.pone.0035691>, 19326203.
- Langer, Max, Pacureanu, Alexandra, Suhonen, Heikki, Grimal, Quentin, Cloetens, Peter, Peyrin, Françoise, 2012b. X-ray phase nanotomography resolves the 3d human bone ultrastructure. *PLoS One* 7 (8).
- Larrue, Aymeric, Rattner, Aline, Laroche, Norbert, Vico, Laurence, Peyrin, Françoise, 2007. Feasibility of micro-crack detection in human trabecular bone images from 3D synchrotron microtomography. Annual International Conference of the IEEE Engineering in Medicine and Biology - Proceedings 3918–3921. <https://doi.org/10.1109/IEMBS.2007.4353190>, 05891019.
- Larrue, Aymeric, Rattner, Aline, Andrei Peter, Zsolt, Olivier, Cécile, Laroche, Norbert, Vico, Laurence, Peyrin, Françoise, 2011. Synchrotron radiation micro-CT at the Micrometer scale for the analysis of the three-dimensional morphology of microcracks in human trabecular bone. *PLoS One* 6 (7). <https://doi.org/10.1371/journal.pone.0021297>, 19326203.
- Launey, Maximilien E., Ritchie, Robert O., 2009. On the fracture toughness of advanced materials. *Adv. Mater.* 21 (20), 2103–2110. <https://doi.org/10.1002/adma.200803322>, 09359648.
- Launey, M.E., Chen, P.Y., McKittrick, J., Ritchie, R.O., 2010a. Mechanistic aspects of the fracture toughness of elk antler bone. *Acta Biomater.* 6 (4), 1505–1514. <https://doi.org/10.1016/j.actbio.2009.11.026>, 17427061, URL.
- Launey, Maximilien E., Buehler, Markus J., Ritchie, Robert O., 2010b. On the mechanistic origins of toughness in bone. *Annu. Rev. Mater. Res.* 40 (1), 25–53. <https://doi.org/10.1146/annurev-matsci-070909-104427>, 1531-7331.
- Le Cann, Sophie, Tudisco, Erika, Turunen, Mikael J., Patera, Alessandra, Mokso, Rajmund, Tägil, Magnus, Belfrage, Ola, Hall, Stephen A., Hanna, Isaksson, 2019. Investigating the mechanical characteristics of bone-metal implant interface using in situ synchrotron tomographic imaging. *Frontiers in Bioengineering and Biotechnology* 6 (JAN). <https://doi.org/10.3389/fbioe.2018.00208>, 22964185.
- Lewis, Robert A., 2004. Medical phase contrast x-ray imaging: current status and future prospects. *Phys. Med. Biol.* 49 (16), 3573.
- Liu, Yahui, Yao, Jian, Lu, Xiaohu, Xie, Renping, Li, Li, 2019. DeepCrack: a deep hierarchical feature learning architecture for crack segmentation. *Neurocomputing* 338, 139–153. <https://doi.org/10.1016/j.neucom.2019.01.036>, 18728286.
- Ma, Shaocheng, Oliver, Boughton, Angelo, Karunarathne, Jin, Andi, Cobb, Justin, Hansen, Ulrich, Abel, Richard, 2016. Synchrotron imaging assessment of bone quality. *Clin. Rev. Bone Miner. Metabol.* 14 (3), 150–160. <https://doi.org/10.1007/s12018-016-9223-3>, 15590119.
- MacDowell, Alastair A., Barnard, Harold, Parkinson, Dilworth Y., Abdel, Haboub, Larson, Natalie, Frank, Zok, Parerai, Francesco, Mansour, Nagi N., Bale, Hrishikesh, Gludovatz, Bernd, Acevedo, Claire, Dong, Liu, Robert, O., Ritchie, 2016. High temperature x-ray micro-tomography. *AIP Conference Proceedings* 1741 (July), 1–5. <https://doi.org/10.1063/1.4952925>, 15517616.
- Maggiano, Isabel S., Maggiano, Corey M., Clement, John G., Thomas, C. David L., Carter, Yasmin, Cooper, David M.L., 2016. Three-dimensional reconstruction of Haversian systems in human cortical bone using synchrotron radiation-based micro-CT: morphology and quantification of branching and transverse connections across age. *J. Anat.* 228 (5), 719–732. <https://doi.org/10.1111/joa.12430>, 14697580.
- Mayo, Sheridan C., Stevenson, Andrew W., Wilkins, Stephen W., 2012. In-line phase-contrast X-ray imaging and tomography for materials science. *Materials* 5 (12), 937–965. <https://doi.org/10.3390/ma5050937>, 1996-1944.
- Mazur, Courtney M., Woo, Jonathon J., Yee, Crista S., Fields, Aaron J., Acevedo, Claire, Bailey, Karsyn N., Kaya, Serra, Fowler, Tristan W., Lotz, Jeffrey C., Dang, Alexis, et al., 2019. Osteocyte dysfunction promotes osteoarthritis through mmp13-dependent suppression of subchondral bone homeostasis. *Bone research* 7 (1), 1–17.
- Milovanovic, Petar, Zimmermann, Elizabeth A., Hahn, Michael, Djonic, Danijela, Püschel, Klaus, Djuric, Marija, Amling, Michael, Busse, Björn, 2013a. Osteocytic canalicular networks: morphological implications for altered mechanosensitivity. *ACS Nano* 7 (9), 7542–7551. <https://doi.org/10.1021/nn401360u>, 19360851.
- Milovanovic, Petar, Zimmermann, Elizabeth A., Hahn, Michael, Djonic, Danijela, Püschel, Klaus, Djuric, Marija, Amling, Michael, Busse, Björn, 2013b. Osteocytic canalicular networks: morphological implications for altered mechanosensitivity. *ACS Nano* 7 (9), 7542–7551. <https://doi.org/10.1021/nn401360u>, 19360851.
- Momose, Atsushi, Kawamoto, Shinya, Koyama, Ichiro, Hamaishi, Yoshitaka, Takai, Kengo, Suzuki, Yoshio, 2003. Demonstration of x-ray talbot interferometry. *Jpn. J. Appl. Phys.* 42 (7B), L866.

- Morgan, Kaye S., Paganin, David M., Siu, Karen K.W., 2012. X-ray phase imaging with a paper analyzer. *Appl. Phys. Lett.* 100 (12), 124102.
- Müller, Ralph, Van Campenhout, H., Van Damme, B., Van Der Perre, G., Dequeker, J., Hildebrand, T., Rüegsegger, P., 1998. Morphometric analysis of human bone biopsies: a quantitative structural comparison of histological sections and micro-computed tomography. *Bone* 23 (1), 59–66. [https://doi.org/10.1016/S8756-3282\(98\)00068-4](https://doi.org/10.1016/S8756-3282(98)00068-4), 87563282.
- Münch, Beat, Pavel Tritic, Federica Marone, Stampanoni, Marco, 2009. Stripe and ring artifact removal with combined wavelet-Fourier filtering. *EMPA Activities* 17, 34–35. <https://doi.org/10.1364/oe.17.008567>, 2009-2010 EMPA ACTIVITIES, 16601394.
- Nalla, R.K., Kinney, J.H., Ritchie, R.O., 2003. Mechanistic fracture criteria for the failure of human cortical bone. *Nat. Mater.* 2 (3), 164–168. <https://doi.org/10.1038/nmat832>, 14761122.
- Nalla, R.K., Kruzic, J.J., Ritchie, R.O., 2004. On the origin of the toughness of mineralized tissue: microcracking or crack bridging? *Bone* 34 (5), 790–798. <https://doi.org/10.1016/j.bone.2004.02.001>, 87563282.
- Nalla, R.K., Kruzic, J.J., Kinney, J.H., Ritchie, R.O., 2005a. Mechanistic aspects of fracture and R-curve behavior in human cortical bone. *Biomaterials* 26 (2), 217–231. <https://doi.org/10.1016/j.biomaterials.2004.02.017>, 01429612.
- Nalla, R.K., Stölken, J.S., Kinney, J.H., Ritchie, R.O., 2005b. Fracture in human cortical bone: local fracture criteria and toughening mechanisms. *J. Biomech.* 38 (7), 1517–1525. <https://doi.org/10.1016/j.jbiomech.2004.07.010>, 00219290.
- Nicoletta, Daniel P., Moravits, Donald E., Gale, Adrian M., Bonewald, Lynda F., James, Lankford, 2006. Osteocyte lacunae tissue strain in cortical bone. *J. Biomech.* 39 (9), 1735–1743.
- Nobakhti, Sabah, Lambert, Georges, Philipp, J., 2014. Turner. Cement lines and interlamellar areas in compact bone as strain amplifiers - contributors to elasticity, fracture toughness and mechanotransduction. *Journal of the Mechanical Behavior of Biomedical Materials* 29, 235–251. <https://doi.org/10.1016/j.jmbm.2013.09.011>, 17516161.
- Nomura, Shintaro, Takano-Yamamoto, Teruko, 2000. Molecular events caused by mechanical stress in bone. *Matrix Biol.* 19 (2), 91–96. [https://doi.org/10.1016/S0945-053X\(00\)00050-0](https://doi.org/10.1016/S0945-053X(00)00050-0), 0945053X.
- Núñez, Juan A., Goring, Alice, Hesse, Eric, Thurner, Philipp J., 2017. Philipp Schneider, and Claire E. Clarkin. Simultaneous visualisation of calcified bone microstructure and intracortical vasculature using synchrotron X-ray phase contrast-enhanced tomography. *Sci. Rep.* 7 (1), 1–9. <https://doi.org/10.1038/s41598-017-13632-5>, 20452322.
- Nuzzo, Stefania, Peyrin, Françoise, Cloetens, Peter, Baruchel, José, Boivin, Georges, 2002. Quantification of the degree of mineralization of bone in three dimensions using synchrotron radiation microtomography. *Med. Phys.* 29 (11), 2672–2681. <https://doi.org/10.1118/1.1513161>, 00942405.
- Nyman, Jeffrey S., Uppuganti, Sasidhar, Makowski, Alexander J., Rowland, Barbara J., Merkel, Alyssa R., Julie, A Sterling, Bredbenner, Todd L., Perrien, Daniel S., 2015. Predicting mouse vertebra strength with micro-computed tomography-derived finite element analysis. *BoneKey Rep.* 4.
- Oftadeh, Ramin, Perez-Viloria, Miguel, Juan, C., Villa-Camacho, Vaziri, Ashkan, Ara Nazarian, 2015. Biomechanics and mechanobiology of trabecular bone: a review. *J. Biomech. Eng.* 137 (1), 1–15. <https://doi.org/10.1115/1.4029176>, 15288951.
- O'Brien, Charles A., Jia, Dan, Plotkin, Lilian I., Bellido, Teresita, Powers, Cara C., Stewart, Scott A., Manolagas, Stavros C., Weinstein, Robert S., 2004. Glucocorticoids act directly on osteoblasts and osteocytes to induce their apoptosis and reduce bone formation and strength. *Endocrinology* 145 (4), 1835–1841. <https://doi.org/10.1210/en.2003-0990>, 00137227.
- Pacureanu, Alexandra, Langer, Max, Boller, Elodie, Paul, Tafforeau, Peyrin, Françoise, 2012. Nanoscale imaging of the bone cell network with synchrotron x-ray tomography: optimization of acquisition setup. *Med. Phys.* 39 (4), 2229–2238.
- Paganin, D., Mayo, S.C., Gureyev, T.E., Miller, P.R., Wilkins, S.W., 2002. Simultaneous phase and amplitude extraction from a single defocused image of a homogeneous object. *J. Microsc.* 206 (1), 33–40. <https://doi.org/10.1046/j.1365-2818.2002.01010.x>, 00222720.
- Palanca, Marco, Tozzi, Gianluca, Cristofolini, Luca, 2016. The use of digital image correlation in the biomechanical area: a review. *International biomechanics* 3 (1), 1–21.
- Palanca, M., Bodey, A.J., Giorgi, M., Viceconti, M., Lacroix, D., Cristofolini, L., Dall'Ara, E., 2017. Synchrotron radiation for microtomography improves the precision of digital volume correlation for bone samples. In: *Orthopaedic Proceedings*, vol. 99. The British Editorial Society of Bone & Joint Surgery, 29–29.
- Peterlik, Herwig, Paul, Roschger, Klaushofer, Klaus, Fratzl, Peter, 2006. From brittle to ductile fracture of bone. *Nat. Mater.* 5 (1), 52–55. <https://doi.org/10.1038/nmat1545>, 14764660.
- Peters, Terry, 1997. CT image reconstruction. *Signal Processing Magazine, IEEE* 14 (1), 67–74.
- Peyrin, F., 2009. Investigation of bone with synchrotron radiation imaging: from micro to nano. *Osteoporos. Int.* 20 (6), 1057–1063.
- Peyrin, Françoise, Dong, Pei, Pacureanu, Alexandra, Langer, Max, 2014a. Micro-and nano-ct for the study of bone ultrastructure. *Curr. Osteoporos. Rep.* 12 (4), 465–474.
- Peyrin, Françoise, Dong, Pei, Pacureanu, Alexandra, Langer, Max, 2014b. Micro-and nano-ct for the study of bone ultrastructure. *Curr. Osteoporos. Rep.* 12 (4), 465–474.
- Qing, Hai, Lynda, F., 2009. Bonewald. Osteocyte remodeling of the perilacunar and pericanalicular matrix. *Int. J. Oral Sci.* 1 (2), 59–65. <https://doi.org/10.4248/ijos.09019>, 16742818.
- Qing, Hai, Ardeshirpour, Laleh, Divieti Pajevic, Paola, Dusevich, Vladimir, Kato, Shigeaki, Wysolmerski, John, Bonewald, Lynda F., 2012. Remodeling in mice during lactation. *J. Bone Miner. Res.* 27 (5), 1018–1029. <https://doi.org/10.1002/jbmr.1567>. Demonstration.
- Raven, Carsten, 1998. Numerical removal of ring artifacts in microtomography. *Rev. Sci. Instrum.* 69 (8), 2978–2980. <https://doi.org/10.1063/1.1149043>, 00346748.
- Reznikov, Natalie, Shahar, Ron, Weiner, Steve, 2014. Bone hierarchical structure in three dimensions. *Acta Biomater.* 10 (9), 3815–3826. <https://doi.org/10.1016/j.actbio.2014.05.024>, 18787568.
- Rho, Jae Young, Kuhn-Spearing, Liisa, Zioupos, Peter, 1998. Mechanical properties and the hierarchical structure of bone. *Med. Eng. Phys.* 20 (2), 92–102. [https://doi.org/10.1016/S1350-4533\(98\)00007-1](https://doi.org/10.1016/S1350-4533(98)00007-1), 13504533.
- Ritchie, R.O., Nalla, R.K., Kruzic, J.J., Ager III, W., Balooch, G., Kinney, J.H., 2006. Fracture and ageing in bone: toughness and structural characterization. *Strain* 42 (4), 225–232. <https://doi.org/10.1111/j.1475-1305.2006.00282.x>, 00392103.
- Ritchie, Robert O., Buehler, Markus J., Paul, Hansma, 2009. Plasticity and toughness in bone. *Phys. Today* 62 (6), 41–47.
- Roschger, Andreas, Roschger, P., Wagermaier, Wolfgang, Chen, Junning, Af van Tol, Repp, Felix, Blouin, S., Berzlanovich, A., Gruber, G.M., Klaushofer, K., et al., 2019. The contribution of the pericanalicular matrix to mineral content in human osteonal bone. *Bone* 123, 76–85.
- Ruiz-Yaniz, Maite, Zanette, Irene, Adrian, Sarapata, Birnbacher, Lorenz, Marschner, Mathias, Chabior, Michael, Olbinado, Margie, Pfeiffer, Franz, Rack, Alexander, 2016. Hard x-ray phase-contrast tomography of non-homogeneous specimens: grating interferometry versus propagation-based imaging. *J. Synchrotron Radiat.* 23 (5), 1202–1209.
- Saban, J., MA, Zussman, Havey, R., Patwardhan, A.G., Schneider, G.B., King, D., 1996. Heterozygous oim mice exhibit a mild form of osteogenesis imperfecta. *Bone* 19 (6), 575–579.
- Salomé, Murielle, Peyrin, Françoise, Cloetens, Peter, Odet, Christophe, 1999. Anne Marie Laval-Jeantet, José Baruchel, and Per Spanne. A synchrotron radiation microtomography system for the analysis of trabecular bone samples. *Med. Phys.* 26 (10), 2194–2204. <https://doi.org/10.1118/1.598736>, 00942405.
- Schlüter, Steffen, Sheppard, Adrian, Brown, Kendra, Wildenschild, Dorthé, 2014. Image processing of multiphase images obtained via X-ray microtomography: a review. *Water Resour. Res.* 50 (4), 3615–3639. <https://doi.org/10.1002/2014WR015256>, 19447973.
- Schmidt, Felix N., Zimmermann, Elizabeth A., Walsh, Flynn, Plumeyer, Christine, Schaible, Eric, Fiedler, Imke A.K., Milovanovic, Petar, Rößle, Manfred, Amling, Michael, Blanchet, Clément, Gludovatz, Bernd, Ritchie, Robert O., Busse, Björn, 2019. On the origins of fracture toughness in advanced teleosts: how the swordfish's sword's bone structure and composition allow for slashing under water to kill or stun prey. *Advanced Science* 1900287. <https://doi.org/10.1002/adv.201900287>, 21983844.
- Schuit, S.C.E., Van der Klift, M., Aeam, Weel, De Laet, C.E.D.H., Burger, H., Seeman, E., Hofman, A., Uitterlinden, A.G., Van Leeuwen, J.P.T.M., Pols, H.A.P., 2004. Fracture incidence and association with bone mineral density in elderly men and women: the rotterdam study. *Bone* 34 (1), 195–202.
- Schweizer, Susanne, Hattendorf, Bodo, Schneider, Philipp, Aeschlimann, Beat, Ludwig, Gauckler, Müller, Ralph, Günther, Detlef, 2007. Preparation and characterization of calibration standards for bone density determination by micro-computed tomography. *Analyst* 132 (10), 1040–1045.
- Seeman, Ego, 2008. Bone quality: the material and structural basis of bone strength. *J. Bone Miner. Metabol.* 26 (1), 1–8. <https://doi.org/10.1007/s00774-007-0793-5>, 09148779.
- Sillence, D.Oetal, Senn, Alison, Danks, D.M., 1979. Genetic heterogeneity in osteogenesis imperfecta. *J. Med. Genet.* 16 (2), 101–116.
- Sinnett-Jones, P.E., Browne, M., Ludwig, W., Buffière, J.Y., Sinclair, I., 2005. Microtomography assessment of failure in acrylic bone cement. *Biomaterials* 26 (33), 6460–6466. <https://doi.org/10.1016/j.biomaterials.2005.04.064>, 01429612.
- Smith, Steven W., 2003. Special imaging techniques. *Digit. Signal Process.* 423–450. <https://doi.org/10.1016/b978-0-7506-7444-7/50062-5>.
- Stampanoni, M., Groso, A., Isenegger, A., Mikuljan, G., Chen, Q., Bertrand, A., Henein, S., Betemps, R., Frommherz, U., Böhrer, P., et al., 2006. Trends in synchrotron-based tomographic imaging: the sls experience. *Developments in X-ray Tomography V* 6318, 63180M.
- Talbot, Henry Fox, 1836. Lxxvi. facts relating to optical science. no. iv. *The London, Edinburgh, and Dublin. Philosophical Magazine and Journal of Science* 9 (56), 401–407.
- Thurner, P.J., Wyss, P., Voide, R., Stauber, M., Stampanoni, M., Sennhauser, U., Müller, R., 2006. Time-lapsed investigation of three-dimensional failure and damage accumulation in trabecular bone using synchrotron light. *Bone* 39 (2), 289–299. <https://doi.org/10.1016/j.bone.2006.01.147>, 87563282.
- Varga, Peter, Pacureanu, Alexandra, Langer, Max, Suhonen, Heikki, Hesse, Bernhard, Grimal, Quentin, Cloetens, Peter, Kay, Raum, Peyrin, Françoise, 2013. Investigation of the three-dimensional orientation of mineralized collagen fibrils in human lamellar bone using synchrotron x-ray phase nano-tomography. *Acta Biomater.* 9 (9), 8118–8127.
- Varga, Peter, Hesse, Bernhard, Langer, Max, Schrof, Susanne, Männicke, Nils, Suhonen, Heikki, Pacureanu, Alexandra, Pahr, Dieter, Peyrin, Françoise, Kay, Raum, 2015. Synchrotron x-ray phase nano-tomography-based analysis of the lacunar-canalicular network morphology and its relation to the strains experienced by osteocytes in situ as predicted by case-specific finite element analysis. *Biomech. Model. Mechanobiol.* 14 (2), 267–282.
- Vidal, F.P., Létang, J.M., Peix, G., Cloetens, P., 2005. Investigation of artefact sources in synchrotron microtomography via virtual X-ray imaging. *Nucl. Instrum. Methods Phys. Res. Sect. B Beam Interact. Mater. Atoms* 234 (3), 333–348. <https://doi.org/10.1016/j.nimb.2005.02.003>, 0168583X.

- Wagner, David W., Lindsey, Derek P., Gary, S Beaupre, 2011. Deriving tissue density and elastic modulus from microct bone scans. *Bone* 49 (5), 931–938.
- Wang, Ji, Kazakia, Galateia J., Zhou, Bin, Shi, X Tony, Guo, X Edward, 2015. Distinct tissue mineral density in plate-and rod-like trabeculae of human trabecular bone. *J. Bone Miner. Res.* 30 (9), 1641–1650.
- Wegst, Ulrike G.K., Bai, Hao, Saiz, Eduardo, Tomsia, Antoni P., Ritchie, Robert O., 2015. Bioinspired structural materials. *Nat. Mater.* 14 (1), 23–36. <https://doi.org/10.1038/nmat4089>, 14764660.
- Weiner, Steve, Traub, Wolfie, Daniel Wagner, H., 1999. Lamellar bone: structure-function relations. *J. Struct. Biol.* 126 (3), 241–255. <https://doi.org/10.1006/jsbi.1999.4107>, 10478477.
- Weitkamp, T., Tafforeau, P., Boller, E., Cloetens, P., Valade, J.-P., Bernard, P., Peyrin, F., Ludwig, W., Helfen, L., Baruchel, J., 2010. Parallel-beam imaging at the esrf beamline id19: current status and plans for the future. In: *AIP Conference Proceedings*, vol. 1234. American Institute of Physics, pp. 83–86.
- Withers, P.J., 2015. Fracture mechanics by synchrotron X-ray microscopy. *Phil. Trans. R. Soc. A* 373:0157 <https://doi.org/10.1098/rsta.2013.0157>.
- Wu, Ziling, Yang, Ting, Deng, Zhifei, Huang, Baokun, Han, Liu, Wang, Yu, Chen, Yuan, Caswell Stoddard, Mary, Li, Ling, Zhu, Yunhui, 2019. Automatic crack detection and analysis for biological cellular materials in X-ray in situ tomography measurements. *Integrating Materials and Manufacturing Innovation* 8 (4), 559–569. <https://doi.org/10.1007/s40192-019-00162-3>, 21939772, URL.
- Yee, Cristal S., Schurman, Charles A., White, Carter R., Alliston, Tamara, 2019. Investigating osteocytic perilacunar/canalicular remodeling. *Curr. Osteoporos. Rep.* 1–12.
- Yeni, Yener N., Norman, Timothy L., 2000. Calculation of porosity and osteonal cement line effects on the effective fracture toughness of cortical bone in longitudinal crack growth. *J. Biomed. Mater. Res.* 51 (3), 504–509. [https://doi.org/10.1002/1097-4636\(20000905\)51:3<504::AID-JBM27>3.0.CO;2-I](https://doi.org/10.1002/1097-4636(20000905)51:3<504::AID-JBM27>3.0.CO;2-I), 00219304.
- Yu, Boliang, Pacureanu, Alexandra, Olivier, Cécile, Cloetens, Peter, Peyrin, Françoise, 2020. Assessment of the human bone lacuno-canalicular network at the nanoscale and impact of spatial resolution. *Sci. Rep.* 10 (1), 1–12.
- Zabler, Simon, Ullherr, Maximilian, Fella, Christian, Schielein, Richard, Oliver, Focke, Zeller-Plumhoff, Berit, Lhuissier, Pierre, DeBoever, Wesley, Hanke, Randolph, 2020. Comparing image quality in phase contrast sub- μ m x-ray tomography—a round-robin study. *Nucl. Instrum. Methods Phys. Res. Sect. A Accel. Spectrom. Detect. Assoc. Equip.* 951, 162992.
- Zhang, W., Liao, S.S., Cui, F.Z., 2003. Hierarchical self-assembly of nano-fibrils in mineralized collagen. *Chem. Mater.* 15 (16), 3221–3226. <https://doi.org/10.1021/cm030080g>, 08974756.
- Zhou, Tunhe, Zanette, Irene, Zdora, Marie-Christine, Lundström, Ulf, Larsson, Daniel H., Hertz, Hans M., Pfeiffer, Franz, Anna, Burvall, 2015. Speckle-based x-ray phase-contrast imaging with a laboratory source and the scanning technique. *Opt. Lett.* 40 (12), 2822–2825.
- Zimmermann, Elizabeth A., Ritchie, Robert O., 2015. Bone as a structural material. *Advanced Healthcare Materials* 4 (9), 1287–1304. <https://doi.org/10.1002/adhm.201500070>, 21922659.
- Zimmermann, Elizabeth A., Launey, Maximilien E., Barth, Holly D., Ritchie, Robert O., 2009. Mixed-mode fracture of human cortical bone. *Biomaterials* 30 (29), 5877–5884. <https://doi.org/10.1016/j.biomaterials.2009.06.017>, 01429612.
- Zimmermann, Elizabeth A., Schaible, Eric, Bale, Hrishikesh, Barth, Holly D., Tang, Simon Y., Reichert, Peter, Busse, Bjoern, Alliston, Tamara, Ager, Joel W., Ritchie, Robert O., 2011. Erratum: age-related changes in the plasticity and toughness of human cortical bone at multiple length scales. *Proceedings of the National Academy of Sciences USA* 108 (35), 14416–14421. <https://doi.org/10.1073/pnas.1107966108>. *Proceedings of the National Academy of Sciences of the United States of America*, 109(29):11890, 2012. ISSN 10916490. doi: 10.1073/pnas.1209596109.
- Zimmermann, Elizabeth A., Busse, Björn, Ritchie, Robert O., 2015a. The fracture mechanics of human bone: influence of disease and treatment. *BoneKEY Rep.* 4 (June), 1–13. <https://doi.org/10.1038/bonekey.2015.112>, 20476396.
- Zimmermann, Elizabeth A., Köhne, Till, Bale, Hrishikesh A., Panganiban, Brian, Gludovatz, Bernd, Zustin, Jozsef, Hahn, Michael, Amling, Michael, Ritchie, Robert O., Busse, Björn, 2015b. Modifications to nano- and microstructural quality and the effects on mechanical integrity in Paget's disease of bone. *J. Bone Miner. Res.* 30 (2), 264–273. <https://doi.org/10.1002/jbmr.2340>, 15234681.
- Zimmermann, Elizabeth A., Schaible, Eric, Gludovatz, Bernd, Schmidt, Felix N., 2016. Christoph riedel, matthias krause, eik vectorazzi, Claire Acevedo, michael hahn, klaus puschel, simon tang, michael amling, robert O. Ritchie, and bjorn Busse. Intrinsic mechanical behavior of femoral cortical bone in young, osteoporotic and bisphosphonate-treated individuals in low- and high energy fracture conditions. *Sci. Rep.* 6 (January), 1–12. <https://doi.org/10.1038/srep21072>, 20452322.
- Zimmermann, Elizabeth A., Riedel, Christoph, Schmidt, Felix N., Stockhausen, Kilian E., Chushkin, Yuriy, Schaible, Eric, Gludovatz, Bernd, Vectorazzi, Eik, Zontone, Federico, Püschel, Klaus, Amling, Michael, Ritchie, Robert O., Busse, Björn, 2019. Mechanical competence and bone quality develop during skeletal growth. *J. Bone Miner. Res.* 1–12. <https://doi.org/10.1002/jbmr.3730>, 00(0), 15234681.
- Zou, Q., Zhang, Z., Li, Q., Qi, X., Wang, Q., Wang, S., 2018. Deepcrack: Learning hierarchical convolutional features for crack detection. *IEEE Transactions on Image Processing* 28 (3), 1498–1512.